Technische Universität München
Lehrstuhl für Elektrische
Energiespeichertechnik
Prof. Dr.-Ing. Andreas Jossen

Performance analysis of packaging geometries of $LiFePO_4$/Graphite (LFPC) cells

Master thesis

of

Ayush Sengupta

Supervisor:
Dipl.-Ing. Ms. Yao Wu

DD. MMMM YYYY

Abstract

Please write a brief abstract before your index.

Following aspects are supposed to be mentioned:

- Briefly describe your motivation/present the problem
- Aims and tasks of the thesis
- Essential results
- If applicable, limitation of the thesis

This paragraph is usually the first page one will see, please be very diligent! The summary shall not be mistaken for the instruction and it should not describe the structure of the thesis.

Abstract

Please also write a brief abstract in English. Same procedure as explained above.

Index

Abrieviation register (Optional)

ESB ..... Ersatzschaltbild

NiMH ..... Nickelmetallhydrid

SOC ..... Ladezustand (engl. state of charge)

Symbol register (Optional)

I_{HL} ..... Hauptreaktionsstrom [A]

I_{NR} ..... Nebenreaktionsstrom [A]

1 Introduction

With the world moving towards consumer electronics, automation and smart technologies, battery energy storage to run these systems have become even more important. Among all, lithium ion battery technologies have found applications from small consumer electronics to large stationary storage systems. Specifically, use of lithium ion batteries is on the rise especially in the case of hybrid vehicles and electric vehicles (HEVs and EVs) with humans consciously attempting to move towards a greener future. Due to its chemical properties, lithium ion can be used in a variety of electrode configuration which makes it an interesting topic of research for the suitability of usage in different applications. The lithium ion batteries used with HEVs and EVs are very expensive making these technologies less affordable. This necessitates the need for further research for reducing costs and optimal functionality. Another important aspect to be taken care of is the safety issues with many of the early lithium ion technologies prone to overheating which not only damages the battery itself but also can be hazardous. The collaborative research project, SPICY aims at development of new generation of Lithium ion batteries with respect to performance, safety, costs, recyclability and lifetime. It particularly involves performance improvement of $LiFePO_4$ based on LFPC cells. $LiFePO_4$ is well known as a safer and more durable cathode material. Unfortunately, its energy density is low due to the electrochemical potential of Fe. One objective of SPICY will be to bind metals having a higher potential than Fe, allowing an increase of the material potential, and thus a higher energy. One of the main objectives in SPICY is to work on the family of polyanionic phosphates bound to metals. This active material allows higher potentials resulting in an increased energy density and reduced battery weight. [1]

The LFPC cells themselves can be available in different packaging geometries: cylindrical, prismatic and pouch. These geometries offer different capabilities with some well-known properties like difference in weight, energy density and packaging efficiencies. Different HEV and EV manufacturers themselves use different packaging geometries for their vehicles. The electric vehicle pioneer, Tesla Motors, uses cells with a cylindrical packaging (traditionally 18650 dimensions and more recently 21700 dimensions). [2] Nissan Leaf and BMW i3 are known to use the prismatic packaged cells. [2] Production ve.hicles such as

Daimler Smart, Renault Zoe and Nissan Leaf as well use cells with pouch type packagaing geometry. [3]

While each design has clear advantages and disadvantages, there is no winner on overall performance for mass-market EVs. [4] Cylindrical cells are still the most matured technology compared to the others. While use of prismatic cells is also on the rise for different battery technologies, pouch cells are only used for the case of Lithium ion cells and was introduced for its reduced weight capabilities. Research has been done for many different commercial cells with respect to their performance, safety and reliability concerns for e.g. the temperature developed or the capacity deterioration mechanism. These also include research on different commercial cells of different geometries. But this does not provide a fair comparison of the performance of the cells in different geometries as the commercial cells researched and compared are either of different chemical composition or have different designed capcities. Dedicated research based on performance and ageing of cells is lacking for the different packaging geometries which have the same chemical composition and are designed to deliver the same capacities. Therefore, the core purpose of the thesis is to analyse cells which are based on the $LiFePO_4$/Graphite electrodes and a design capacity of 16 Ah but differ only in their packaging geometries and the results of which should in logically be comparison of the packaging geometries. As a long term scope, the results can help further research which may eventually determine the suitability of one geometry for particular applications as compared to the others.

During the course of the thesis, the data was obtained from various tests performed by different partner organizations of the SPICY project, as mentioned earlier. State of the art methods were used for the cell manufacture itself and care was taken to maintain uniformity with respect to chemistry and capacity sizing of the various geometries for a fair comparison. The data obtained was then sorted, analysed and visualized using softwares like EC-Lab and MATLAB. Several assumptions were made across the cell analysis for ease of comparison and data visualization. Further, the experimental results were attempted to be validated or inference were made based on previous research by peers.

The thesis is arranged into different chapters. First, the basics of Lithium ion technology is discussed especially with respect to $LiFePO_4$/Graphite based cells and a discussion on the different geometries of packaging and the existing knowledge about their comparison. The next chapter discusses the state of the art in the research on performance analysis of the geometries of the cell. It also includes a discussion of the literature on the performance and ageing mechanism evaluators of Lithium ion cells, especially those relevant to the thesis work. In the subsequent chapter, the different cells used during the experiments are described followed by detailing the specific experiments setup. This is followed by discussion

of the experiment results and inference based on the literature review done before. The core part of the thesis ends with a conclusions drawn from the results, a discussion on limitations within the work and the scope for future research and improvements.

2 Lithium ion batteries and packaging geometries

In this chapter, a brief introduction has been made about the Lithium ion battery technology in general, followed by a discussion of the $LiFePO_4$/Graphite based cells and an introduction to the packaging geometries. This chapter serves as the knowledge foundation for the rest of the work.

2.1 Lithium ion technology

Lithium ion batteries play a significant role in present day energy storage systems, primarily due to their high energy density and high specific energy. Invented by the American physicist Professor John Goodenough in 1980 as a new type of battery in which the lithium (Li) could migrate through the battery from one electrode to the other as a Li^+ ion, it was first commercially introduced as a product by Sony Corporation. [5]; [6] The simple basis of these batteries is that a compound of lithium with a transition metal - such as nickel, manganese, cobalt, iron - and oxygen forms the cathode, whereas, graphite is the anode. [5]

In terms of chemistry, Lithium ion cells have several advantages over other technologies. Due to its lowest reduction potential of all elements, Lithium ion cells have the highest available cell potential. Further, because of being one of the lightest element and having one of the smallest radii, Li-based batteries have high gravimetric and volumetric capacity and power density. [7] Therefore, despite disadvantages like high costs and possible high temperature development, the above advantages make it very desirable for many commercial and research-related activities. This prompts for further studies and experiments to improve safety and reducing the costs of Lithium ion batteries.

The properties of lithium and the diversity of lithium-ion cells make them more suitable for battery technologies than various other technologies. Lithium ion batteries are made of lightweight lithium and carbon, making it lighter than other types of rechargeable batteries of the same type. Lithium itself is highly reactive and has potential to store high energies. Lithium ion batteries hold their charge for longer periods of time, that is they have low self-discharge. No memory effect, which means that Lithium ion batteries do not have to be completely discharged before recharging to retain full charge capacity, which is the case in some battery chemistries like NiCd. Lithium ion batteries have long cycle lives and can retain large number of charge-discharge cycles without significant losses in capacity. [8]

However, lithium ion cells have a few disadvantages as well. The service life or shelf life of a Lithium ion battery decreases with aging even if it is not used unlike other chemistries. This means that from the time of manufacturing, regardless of the number of times it was cycled, the capacity of a Lithium ion battery will decline gradually. This is due to an increase in internal resistance, which makes the problem more pronounced in high-current applications than low-current ones. They are more sensitive to high temperatures than most other chemistries. Hot storage and operating conditions causes Lithium ion battery packs to degrade much faster than they normally would. Lithium ion batteries can be severely damaged by deep discharge, i.e., by discharging them below the minimum voltage threshold recommended by the manufacturer (usually 2.7 V for a single cell). Consequently, Lithium ion battery packs come with an on-board circuit to manage the battery. This makes them even more expensive than they already are. In general Lithium ion chemistry is not as safe as NiCd or NiMH. This is because the anode produces heat during use, while the cathode produces oxygen (not for all Lithium ion chemistries). Lithium being highly reactive can combine with this oxygen, leading to the possibility of the battery catching on fire. [8]

Table 2.1 shows a comparison of Lithium ion batteries with other technologies.

Cathode	**Lithium ion**	**Pb-acid**	**Ni-Cd**	**Ni-MH**
Cycle life	500-1000	200-500	500	500
Working potential (V)	3.6	1.0	1.2	1.2
Specific energy (Wh/kg)	100	30	60	70
Specific energy (Wh/L)	240	100	155	190

Table 2.1. Comparison of different battery technologies [9]

Currently, Lithium ion technologies are used in a variety of applications, especially in portable electronics, hybrid/electric vehicles and power tools. The high energy efficiency of Lithium ion batteries may also allow their use in various electric grid applications, including improving the quality of energy harvested from wind, solar, geo-thermal and other renewable sources, thus contributing to their more widespread use and building an energy-sustainable economy. [7]

Because of Li's ability to form compounds with a variety of transition metals and oxygen, different types of Li battery technologies are available. Table 2.2 shows some typical properties and their applications of the most commonly used types of Lithium ion batteries:

	Li-Cobalt (LCO)	**Li-Manganese (LMO)**	**Li-Nickel Manganese Cobalt (LNMC)**	**Li-Iron Phosphate (LFP)**
Specific energy (Wh/kg)	150-200	100-150	150-220	90-120
Nominal voltage (V)	3.6	3.7	3.7	3.3
Cycle life	500-1000	300-700	1000-2000	1000-2000
Cost (USD/kWh)	-	-	420	580
Application	Mobile phones, tablets, laptops, cameras	Power tools, medical devices, electric powertrains	E-bikes, medical devices, EVs, industrial	Portable and stationary needing high load currents and endurance

Table 2.2. Typical properties and applications of some main types of Lithium ion cells [10]

The advantages of lithium ion batteries far outweigh the disadvantages in terms of commercial application capabilities which necessitates the need for research to understand and alleviate the shortcomings of the technology and perfect. Such research work led to the development of $LiFePO_4$/C (or more commonly, LFPC) cells which is known to be low cost and offers safety, stability and well-defined performance. LFPC cells form the basis of studies in this thesis work. The next sub-section introduces and discusses a typical LFPC cell, its geometry and chemistry in general.

2.2 $LiFePO_4$/Graphite cells

John B. Goodenough research group at the University of Texas first published a literature in 1996 about the use of $LiFePO_4$ as an electrode for Lithium ion cells. [11] With a specific capacity compared to other technologies and a well-defined performance, LFPC cells have found application in EV-HEVs, stationary storage systems, power backup systems among others. [12] Despite disadvantages like low electrical conductivity and slow Li-solid state diffusion and therefore, low specific energy and low capacity, LFPC is one of the safest Lithium ion technologies. It consists of $LiFePO_4$ as the cathode along with a graphitic carbon electrode in a metallic current collector grid as the anode. $LiFePO_4$ based cathodes, while having less energy density, have larger power density and better longevity as comapred to other cathodes. [13] To further discuss the chemistry of LFPC cells, Figure 2.1 introduces a schematic of the ion-transport in the cell.

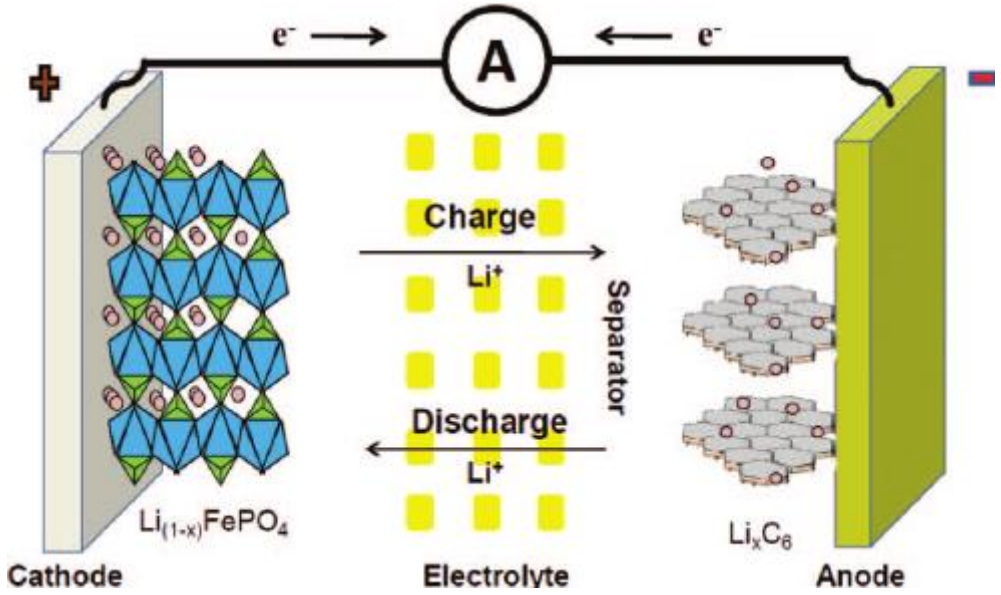

Figure 2.1. Schematic of ion-transport in a $LiFePO_4$/C cell [14]

Each LFPC battery consists of an anode of graphite on copper terminals and a cathode of $LiFePO_4$ on aluminium terminals separated by an electrolyte containing dissociated lithium salts like $LiPF_6$ in ethylene carbonate (EC)/dimethyl carbonate (DMC), which enables transfer of lithium ions between the two electrodes. [13] [14] The separator isolates the two electrodes and is a membrane that allows transfer of ions from cathode to anode on charge (reverse on discharge). The small current passing through the separator constitutes the self-discharge and gradually reduces the cell capacity.

Equation (2.1) below represents the general chemical reaction in a $LiFePO_4$ based cell. While the forward process shows the extraction of Lithium ion to charge the cathode, the reverse process shows the discharge phenomenon. [9]

$$LiFePO_4 - x\,Li^+ + -x\,e^- \leftrightharpoons x\,FePO_4 + (1-x)\,LiFePO_4 \quad (2.1)$$

The chemical reaction has been broken down to part reactions in the following table :

$LiFePO_4 \leftrightharpoons FePO_4 + Li^+ + e^-$		$Li^+ + e^- + 6C \leftrightharpoons LiC_6$
Cathode ($LiFePO_4$ on Al terminal)	**Electrolyte** $LiPF_6$ in ethylene carbonate (EC)/ dimethyl carbonate (DMC)	**Anode** (Graphite on Cu terminal)
Left to right → Charging		Right to left ← Discharging

Table 2.3. Part reactions involved in the chemistry of an LFPC cell [13]

Table 2.3 helps understand the part reactions taking place at each of the electrodes during charging and discharging, which is essential to explain the ion-electron movement across the cell and related electrochemical processes and resistances involved.

2.3 Packaging geometries of Lithium ion cells

The main aim of this thesis is to compare the different packaging geometries of Lithium ion cells. Most large secondary batteries come in either prismatic or cylindrical configurations, while pouch type configuration is also present in the case of Lithium ion cells. In this sub-section, a brief introduction and a comparison of the geometries is made. Figure 2.2 below shows components of the different geometries of Lithium ion cells.

Cylindrical geometry is the most common packaging technique for both primary and secondary cells. It has the main advantages of ease of manufacture and good mechanical stability. The tubular cylinder can withstand high internal pressures without deforming. Even

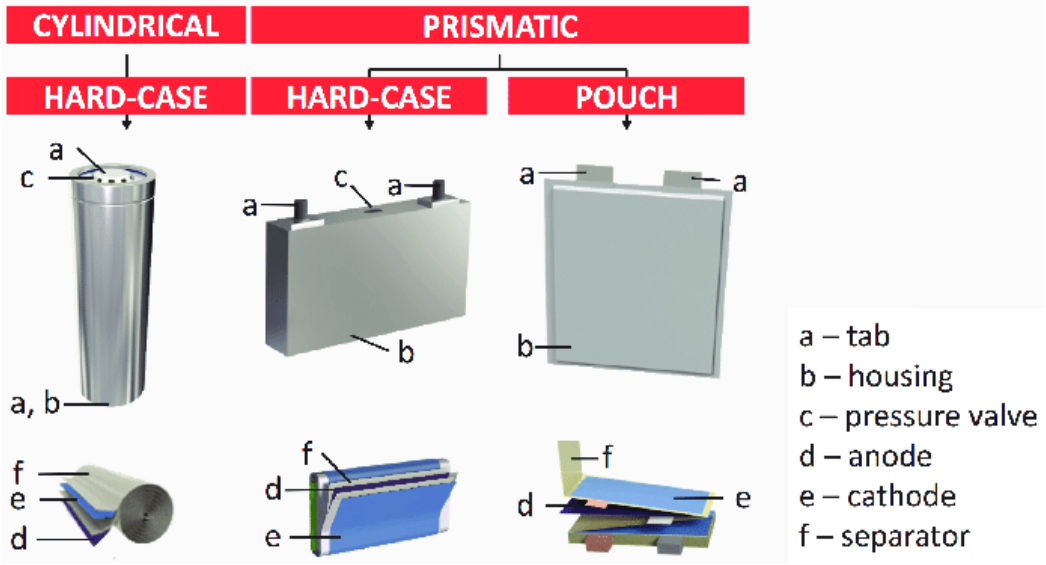

Figure 2.2. Diagram showing different geometries of Lithium ion batteries [15]

though the cylindrical cell does not fully utilize the space by creating air cavities on side-by-side placement, among all the commercial cells available today in the market, cylindrical cells are the most matured technology and provide the highest energy density. The higher energy density of the cylindrical cell compensates for its less ideal stacking abilities and the empty space can always be used for cooling to improve thermal management. This cell design allows for added safety features that are not possible with other formats. It cycles well, offers a long calendar life and is low cost, but it has less than ideal packaging density. It is available in several different geometrical sizes, with the 18650 type being the most popular. The nomenclature 18650 refers to an 18mm diameter, a 65mm height, while the last 0 refers to a cylindrical cell conforming to the IEC standards. The other Lithium ion formats commonly available commercially are 20700, 21700 and 22700. It has been estimated that in the future pouch cells will become cheapest to manufacture. [16]

Prismatic cells are encased in aluminum or steel for stability. Jelly-rolled or stacked, the cell is space-efficient but can be costlier to manufacture than the cylindrical cell. The prismatic cell improves space utilization and allows flexible design but it can be more expensive to manufacture, less efficient in thermal management and have a shorter cycle life than the cylindrical design. [16]

The pouch cell offers a simple, flexible and lightweight solution to battery design. Some stack pressure is recommended but allowance for swelling must be made. The pouch cells can deliver high load currents but it performs best under light loading conditions and with moderate charging. It is cost-effective but exposure to humidity and high temperature can

shorten life. Adding a light stack pressure prolongs longevity by preventing delamination. Swelling of 8–10 percent over 500 cycles must be considered with some cell designs. [16]

It has already been discussed that cylindrical cells are used in Tesla Motors electric vehicles, while prismatic cells are common in BMW i3 and pouch type geometry are used Daimler Smart and Renault Zoe. The following three figures show the arrangements of these geometries into battery packs in different EV-HEV cars.

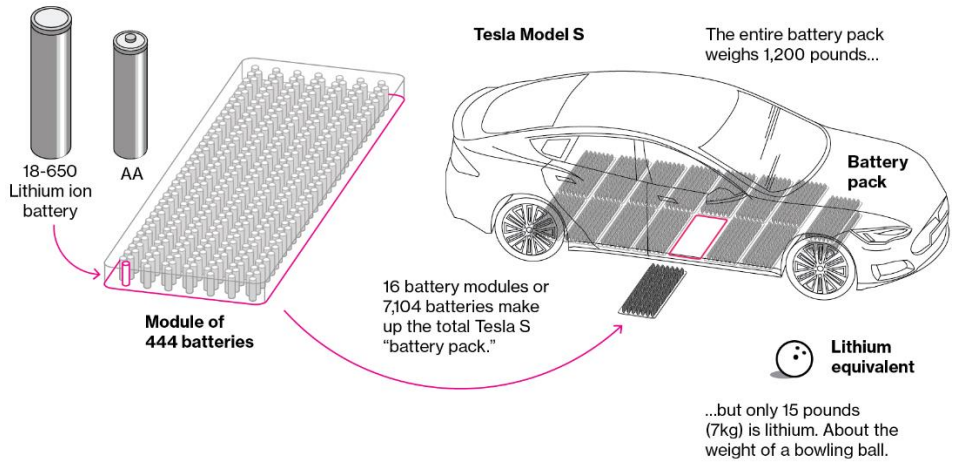

(a)

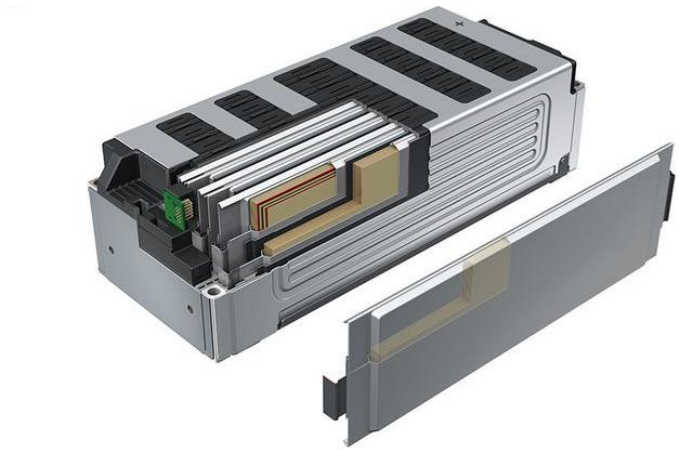

(b)

(c)

Figure 2.3. Battery pack arrangement for (a) Cylindrical [17], (b) Pouch [18], (c) Prismatic cells [18]

Figure 2.3a shows a diagram of a 18650 cylindrical cell battery pack for the Tesla S model. Figure 2.3b and Figure 2.3c show the pouch and prismatic cell battery packs ehich are being developed by AUDI for their future electric cars. While the cylindrical cells leave behind some space from one cell to another due to their cylindrical shape, prismatic and pouch geometries show a more compact packaging, with the thin pouches providing scope for more flexibility.

While use of these geometries in different electric and hybrid-electric vehicles has already been discussed, they find different applications in other fields as well. Cylindrical cells mostly find use in portable applications and are used in power tools, medical instruments, laptops and e-bikes. Prismatic cells are popular in Mobiles phones, tablets and low-profile laptops electric powertrains, solar/wind storage UPS. Pouch cells are also used portable applications like drones and hobby gadgets and also in energy storage systems (ESS). Standardised pouch cells are not available and it gives the manufacturers the flexibility to design to their specific needs. [19] Each cell geometry has its own pros and cons in each application but currently, the scope itself is limited by the maturity of technologies with cylindrical cells being the most advanced and researched.

Table 2.4 on the next page summarizes the advantages and disadvantages of each type of cell geometry.

Cylindrical	**Prismatic**	**Pouch**
+ Ease of manufacture + Good mechanical stability + Withstand high internal pressure without deforming + Lower cost (watt per hour) + Long calendar life and cycling ability + Higher energy density	+ Thin profile (effective use of space) + Allows flexible design + Encased in metal or steel for stability	+ No need for metallic casing + Most efficient use of space + Light weight
- Notable space between cells (less space efficiency) - Heavy - Low packaging density due to space cavities	- Expensive to manufacture - Less efficient in thermal management - Shorter cycle life - Deforms at high pressure - Higher cost (watt/hour)	- Provision for swelling must be made - Cons like prismatic structure

Table 2.4. Comparison of cell packaging geometries

3 State of the Art

Lithium-ion cells are taking over the storage market from low power to high power applications. As discussed already, due to the chemical properties of lithium, these cells can be produced with many different configurations of cathodes and anodes and in various sizes. There is further evidence in benefits of using $LiFePO_4$ based cathodes and its increasing importance. Many studies have been done to compare the different chemistries of Lithium ion cells and even different sizes in terms of geometries.

On the other hand, studies on the packaging geometries of the Lithium ion cells are limited. Pouch based packaging geometries, for e.g., are finding lot of applications in EVs and HEVs and are even replacing cylindrical cells in many cases because the improved energy density and low weight due to its lightweight outer covering. Very few studies include a thorough comparison based on its performance analysis with respect to parameters like capacity evolution, internal resistance developed, differences in chemical changes during cycling, among others. This chapter discusses the state of the art in research for the comparison study between the cell packaging geometries. The literature reviewed in this study is not just limited to LFPC and Lithium ion cells, but tries to incorporate relatable results from the work on other electrochemical cells as well.

3.1 Literature review on packaging geometry comparison

A physical and geometrical comparison of the three packaging types can be found in the work done by Lee et al. It compares the physical constraints of jelly roll wound types (cylindrical and prismatic) with flat stacked designs (pouch) for Lithium-polymer cells. In the case of jelly roll configurations, the metal enclosure of slimmer batteries (for e.g. prismatic cells) do not exert enough pressure onto the electrodes and results in poor thickness control. It also enumerates some of the advantages of a flat design: maintaining uniform battery thickness, higher energy densities due lower dead volume and lower cell impedance due to the plurality of electrical contacts through electrode tabs. Further, free stack structures without any folding options, which specifies the pouch type cells, allow the separator materials to contract when exposed to shutdown temperatures, which results in triggering safety events more easily around the electrode edges. The work illustrates the need for studying of cell designs for safer lithium ion battery technology. [20]

The work by Maiser gives a brief overview of battery packaging concepts, their specific advantages and drawbacks, as well as the importance of packaging for performance and cost. It concludes that while the front-end production have the highest impact on the cost of the battery, back-end design and processing (packaging) adds important safety and

intelligent control features without which Lithium ion batteries would not be manageable. It also reviews a brief history, characteristics and applications of the three packaging geometries relevant to this work: cylindrical, prismatic and pouch. [21]

Mulder et al. have done a comprehensive study on the comparison of commercial Lithium ion battery technologies with different chemistries and packaging geometries. The work evaluates the behavior of these cells for automotive applications like plug-in hybrid vehicles and battery electric vehicles, where tests for high power and high energy applications are included. Within the scope of this study, commercial cells of different geometries were also studied and a comparison was made. It was concluded that pouch cells behave better than average with respect to the power efficiency, whereas due to design factors, the prismatic shape has a clear negative effect on the efficiency. Prismatic cells also seem to have a clear negative effect on efficiency, as it becomes the hottest, while cylindrical cells warm up less. Further, pouch cells show the highest power densities. While this work is comprehensive and includes many parameters for comparison, it does not necessarily include whether the cells from the three packaging geometries have the same internal chemical composition and design capacities. [22]

Further literature studied for this work involved studies on capacity evolution, aging parameters, internal resistances, temperature developed and pulse polarization tests of Lithium-ion cells. The following part discuss in detail the various aspects related to capacity deterioration and overpotentials along with the associated resistances.

3.2 Capacity deterioration

The cyclic ageing and capacity deterioration of Lithium ion cells depends on a variety of factors as enumerated by Zhao: loss of lithium ion-inventory, loss of active material, ohmic resistance increase, lithium plating among others. [23] These mechanisms are discussed further in detail by González. [24] Barré et al. have reviewed the ageing mechanism, and ageing battery estimation methods in Lithium ion batteries. [25] Sarasketa-Zabala et al. provide a detailed analysis of the influence of DOD, C-rate and Ah-throughput on cell ageing of LFPG cells. [26] Pinson discusses the theory of solid electrolyte interface (SEI) in rechargeable batteries: capacity fade, accelerated aging and lifetime prediction. [27]

Many literatures study the ageing characteristics of Lithium ions cells and discuss the involved mechanisms, although the mechanisms may differ from one chemistry and cell geometry to other. The work done by Sikha et al. discusses the capacity fade of cylindrical 18650 Lithium ion cells at different charge-discharge protocol. For the constant current –

constant voltage (CC+CV) and constant voltage (CV) protocol, that has been used in this thesis work, the short time during which the current is very high while charging using CV protocol is responsible for increased capacity fade. [28] Most of the known work in the case of understanding the ageing behavior is done for the case of commercial cylindrical cells. Han et al. investigated different commercial Lithium ion cells and concluded that the ageing mechanism differ with different chemistries of the cells. Two LFPC cells were investigated in this study and it was observed that the battery aging mainly arises from the loss of lithium inventory and loss of the anode active material, while in another case despite lithium inventory loss, no significant anode or cathode loss was observed. [29] Sun et al. studied the degradation mechanism with respect to the cycle lifetime of commercial $LiFePO_4$/Graphite cells at different ambient temperatures and observed that the mechanism changes for different temperatures. While at room temperatures, the capacity fade is due to active lithium loss by generation and reformation of solid electrolyte interface (SEI) film, at temperatures above 35°C, the electrolyte decomposes which results in accelerated consumption of active lithium. Elevated temperatures have an adverse influence on the performance of $LiFePO_4$ material. [30] Further many literatures have explored the use of differential voltage analysis (DVA) to studying aging. One such study, Lewerenz et al, uses DVA for calendar and cycling ageing of cylindrical LFPC cells and focusses on mechanisms of homogeneity of active lithium distribution and loss of active anode material. They arrive at the conclusion that for cycling ageing, several phenomena are correlated to degradation, such as loss active lithium, local loss of active anode material for depth of discharge (DOD) 100%, deactivation of certain layers of anode and cathode due to a lithium-permeable covering layer on top of the anode. [31]

The literature review of the ageing in different cells revealed many different trends for different cells. Despite that not much work has been done for the distinction of ageing among Lithium ion cells based on packaging geometries (cylindrical cells being the most popular geometry for research). But the different mechanisms of ageing have been well researched and as discussed above can be mainly categorized as loss of lithium inventory (LLI), loss of active material (LAM), ohmic resistance increase (ORI) and lithium plating. As discussed in the next paragraphs, these mechanisms are interrelated and are tailored around the SEI layer formation and disruptions in it. The next subsection briefly discusses the concept of SEI layer formation, its importance for the cell ageing and the different ageing mechanisms

3.2.1 SEI layer formation

During the first charging cycle of a Lithium ion cell, a passivation film builds on graphite/electrolyte interface. When the charging process starts, Li^+ ions travel through the

electrolyte towards the graphite anode. Some Li^+ ions react with the degradation products of the electrolyte and form insoluble parts that deposit on the anode. Slow charging results in densely packed SEI layer which prevents graphite structure from decomposition. Then the SEI layer strips off the solvent molecules aurrounding the Li^+ ions. Additionally, the SEI layer prevents the anode lattice from exfoliation and in an ideal case, allows cycling of lithium batteries without major capacity fades (except for the initial capacity drop loss due to losing lithium inventory to SEI layer fomation). [32] It is vital to the performance of the lithium ion cell, since the entirety of the anode must have a uniform layer of SEI to prevent further disintegration of the electrolyte. [20]

An optimized SEI layer is expected to have negligible electrical conductivity, high electrolyte diffusion resistance while having high lithium selectivity and permeability. Once it is properly formed, further decomposition reactions with salts and solvents are prevented as electrons cannot transfer to or through the layers. Properties of an ideal SEI formation are high electrical resistance, high lithium selectivity, high strength, tolerance to expansion and contraction stresses. [20]

In real cases, the SEI-layer thickens by repeated cycling gradually due to electron exposure to electrolyte and electrolyte diffusion to graphite surface. This not only leads to electrolyte decomposition but also might lead to loss of active lithium. [20] The most common and fundamental source of capacity fade in successful Lithium ion batteries (which manage to resist degradation over hundreds of cycles) is the loss of lithium to the solid-electrolyte interphase (SEI), which typically forms at the negative electrode during recharging. [27] Four different ageing mechanisms attempt to explain various ways in which this can happen.

3.2.2 Ageing mechanisms

Four major ageing mechanisms are studied by most literatures to account for the the capacity fade in Lithium ion batteries which are namely: loss of lithium inventory (LLI), loss of active material (LAM), ohmic resistance increase (ORI) and lithium plating. Often these mechanisms are inter-related as discussed in this section.

Loss of lithium inventory (LLI) leads to loss of Li ions due to parasitic reactions, though it does not change the content of active materials in electrodes and their properties. It is reported to be the major cause of degradation of lithium-ion batteries. It is attributed to two main causes: the primary cause is the SEI layer formation, growth and destabilization, and the secondary cause of side reactions of lithium ion with decomposed electrolyte compounds and water in the electrolyte. LLI occurs chiefly at the electrode/electrolyte interface and is

predominant on the negative electrode where SEI formation dominates. SEI growth and subsequent LLI is dependent on temperature: at high temperatures, the SEI either grows in thickness or becomes non-protective leading to performance degradation, whereas at low temperatures, the risk of lithium plating leads to cell degradation. [24]

Loss of active material (LAM) directly affects the structure of the electrodes, reducing the volume of active material used in the cell and the ageing effects in this case are more prominent in graphite based negative electrodes than positive electrodes. It is enhanced by high currents, high temperatures and high SOC. The major reasons of LAM are: particle isolation, side reactions within the active material of the electrodes and physical degradation. LAM may lead to second stages of cell degradation where abrupt capacity losses might appear after steady capacity loss in the first stage. [24]

In ohmic resistance increase (ORI), degradation caused on the electrodes and electrolyte materials directly result in the increase in the electronic and ionic resistances, respectively. The possible reasons for ORI are particle isolation causing LAM, binder decomposition, current collector corrosion, volume changes in active material and electrolyte contamination, SEI growth, destabilization affecting ionic resistance. [24]

Lithium plating occurs during charging when lithium ions deposit on the negative electrode instead of intercalating into the graphite. It is the most detrimental aging mechanism as it also leads to safety deterioration. It can result from large number of factors, like constructive properties of the cell to operating conditions (like low operating temperatures and high current rates). Li plating increase LAM and LLI. It is initiated by strenuous charges, charging at low temperatures, cell constructive design or conventional aging of the cell. [24]

One of the major consequence of ageing is the changes in the internal resistance of the cell, mostly an increase, and the next subsection studies the overpotentials and realted internal resistances involved.

3.2.3 Internal resistances and overpotential

In this thesis work, the internal resistance have been measured through 30s pulse (charging and discharing test) which will be further discussed in the next chapter. To understand and analyse the results from the pulse tests, this section discusses the concept of overpotentials and internal resistances. It starts with a brief literature review of the concepts and then a further in-detail discussion.

The purpose of the pulse tests is to reproduce a polarization curves at different state of charge (SOC) of the cells. Polarization curves are a popular way to study the behavior of a cell during operation. DuBeshter [33] has discussed a way to develop pulse polarization curves (PPC) for a Lithium ion battery under constant SOC to identify individual over-voltages, such as charge transfer kinetics and mass transport, and their SOC dependence. In this work, different time scales of a discharge pulse have been formulated to represent the kinetic overpotential, electrolyte Li^+ concentration and Li solid state diffusion.

Liu et al. [34] have studied the differences in electrochemical potentials in different rechargeable batteries. Lithium ion batteries are always accompanied by solid-state mass diffusion as well as volume expansion or contraction, although the electrode surfaces do not recede or advance when the volume change of electrodes is not considered. While the concentration of lithium ions remains constant in the electrolyte regardless of the degree of charge or discharge, it varies in the cathode and anode with the charge and discharge states. Liu et al [34] further summarize that an SEI film permits the diffusion of Li ions through the film under a uniform electric field and reduces the overpotential and concentration polarization. The SEI can also prevent the aggregation of electrochemically active particles and maintain a uniform chemical composition at the electrodes.The SEI film increases the internal resistance of the battery and consumes part of the Li ions from the cathode, leading to both power and capacity loss. This helps in correlating the SEI film formation with both the polarization process, internal resistance increase and capacity losses.

Saha and Goebel [8] have done a study on the modeling of Lithium ion battery capacity depletion in a particle filtering framework and have further described the battery characteristics and the concept of overpotential in their work. Park et al. [35] have done a review of the conduction phenomena in Lithium ion batteries and have explained the term polarization curve. The cell potential is calculated as the difference of the Gibbs free energies the product of the reactants and products (potential difference between the electrodes), with the theoretical open circuit voltage, E^o, measured with the reactants at 25°C and 1M solutions. This is the equilibrium potential. But during the operation of the battery, due to current flow or charge flow, the potential deviates from the equilibrium and this shift is known as the polarization. In the case of oxidation (loss of electrons), the actual potential is more than the equilibrium potential, while the vice-versa is true for reduction (gain of electrons). This shift or voltage drop is due to various passive components inside the electrolyte, the separator, the terminal leads etc., which are characterized as the following factors [8]:

- Internal resistance (IR) drop: Voltage drop associated with the internal resistance of the battery during the current flow across the terminals. The internal resistance has been categorically divided in Table 3.1.
- Activation polarization: This involves the kinetics involved with the electrochemical reaction, like the work function that the ions must overcome at the junction between the electrodes and electrolytes. It is associated with the kinetics of charge transfer.
- Concentration polarization: The potential drop associated with the mass transfer resistance (e.g. diffusion) during the ion transportation across the electrolyte from one electrode to another. It is associated with the kinetics of mass transfer.

This can be mathematically denoted using the equation (3.1):

$$E = E_0 - [(\Phi_{ct})_a + (\Phi_{ct})_c] - [(\Phi_c)_a + (\Phi_c)_c] - iR_i = iR \tag{3.1}$$

where, E_0 is the standard cell potential, $(\Phi_{ct})_a$, $(\Phi_{ct})_c$ are activation polarizations (charge-transfer over voltage) at the anode and cathode, $(\Phi_c)_a, (\Phi_c)_c$ are concentration polarizations at the anode and cathode, i is the cell operating current, R_i is the internal resistance of the cell and R is the apparent cell resistance.

Zhang Zhou et al. [36] have studied different dynamic phenomena inside the battery: lithium-ion migration through the solid electrolyte interface (SEI) layer, activation kinetics in both negative and positive electrodes, double layer effects at the interfaces of electrolytes, and lithium-ion diffusion processes in the active material of the electrodes. They also discussed the overpotentials and resistances related to the various sections of the reaction cell by performing the electrochemical impedance spectroscopy (EIS). This can be explained using the Figure 3.1. The different regions correspond to different internal resistances and chemical phenomena. Region A can be represented by single ohmic resistance, R_o, and includes resistances of the current collector, active material, electrolyte and separator. Region B represents the SEI layer resistance (R_{sei}) – characterized by a high frequency. Region C (medium frequency) represents the charge transfer resistance (R_{ct}). The low frequency region, D, represents the lithium-ion diffusion process in the active material of the electrodes. [36]

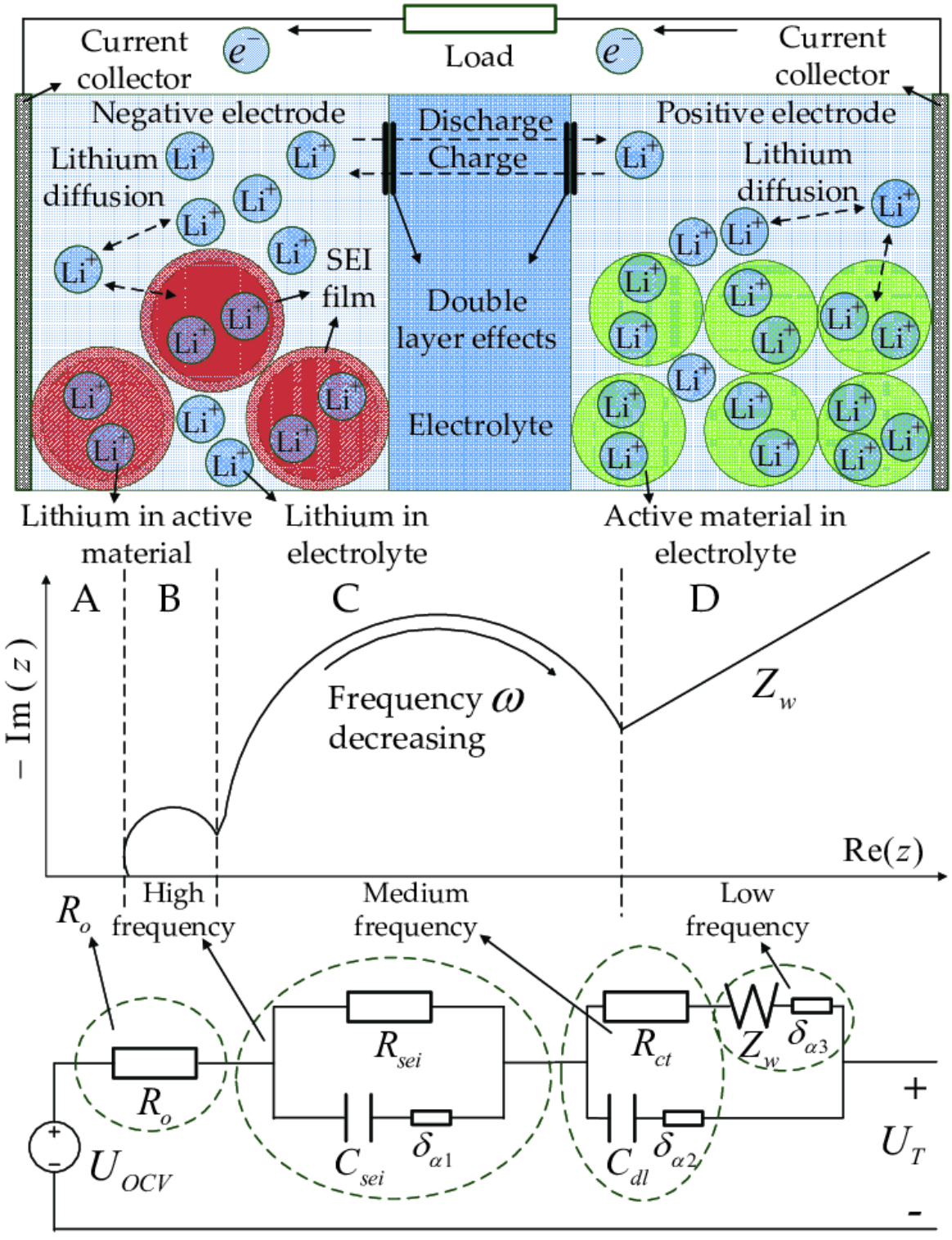

Figure 3.1. Lithium ion battery internal dynamic phenomena, and equivalent impedance circuit.

The internal resistance of a cell as studied from the literature review above can be summarized as shown in Table 3.1 below:

Type of resistance	**Internal resistance of cell, R_i=ionic resistance + electrical resistance + interfacial resistance**
Ionic	• Electrode particle • Electrolyte
Electrical	• Electrode particle • Conductive additives • Percolation network of additives in electrode • Current collectors • Electrical taps
Interfacial	• Between electrolyte and electrodes • Between electrode particles and conductive additives • Between electrode and current collectors • Between conductive additives and current collectors

Table 3.1.Types of internal resistances [35]

Further, Park et al [35] have reviewed the electrical and ionic conductivity separately for anodes and cathodes, especially with interesting insights into $LiFePO_4$ based cells. Assuming diffusion governs charge/discharge rates, ionic conductivity is more significant than electronic conductivity because high ionic conductivity will allow rapid diffusion of Lithium ions into the cathode materials in the case of charging. Conduction in graphite anodes is complex due to the continuous phase transformations and the formation of SEI layers. A prominent feature of graphite anodes is the staged intercalation of Lithium ion, and the diffusivity of Lithium ions in graphite is found to be a function of intercalation or electrical voltage. [35] It is concluded that major features of conduction in the anode are closely related to phase transformations as a function of Lithium ion intercalation and SEI layer formation.

A typical charge-discharge curve of a lithium ion battery is represented in the Figure 3.2. In order to locate the different regions of a polarization curve based on the cell chemistry, DuBeshter and Jorne [33] have designed a method adapt polarization curve from fuel cells to Lithium-ion batteries in order to understand the governing factors of battery performance under various operating conditions at different SOCs The polarization curve here can be divided into three parts, namely, (a) the activation part representing the kinetic region, (b) the ohmic part representing the ionic exchange, and (c) the concentration part representing the mass-transfer region. The adapted method can be used to give information about the charge transfer kinetics, ionic mass transport and solid-state diffusion. According to this method, for the pulse test, different time instants of the pulse represents different parts of the three governing factors. To create pulse polarization curve using this method, the end SOC must remain constant and that is the reason why the pulse test in this thesis is performed at a constant SOC.

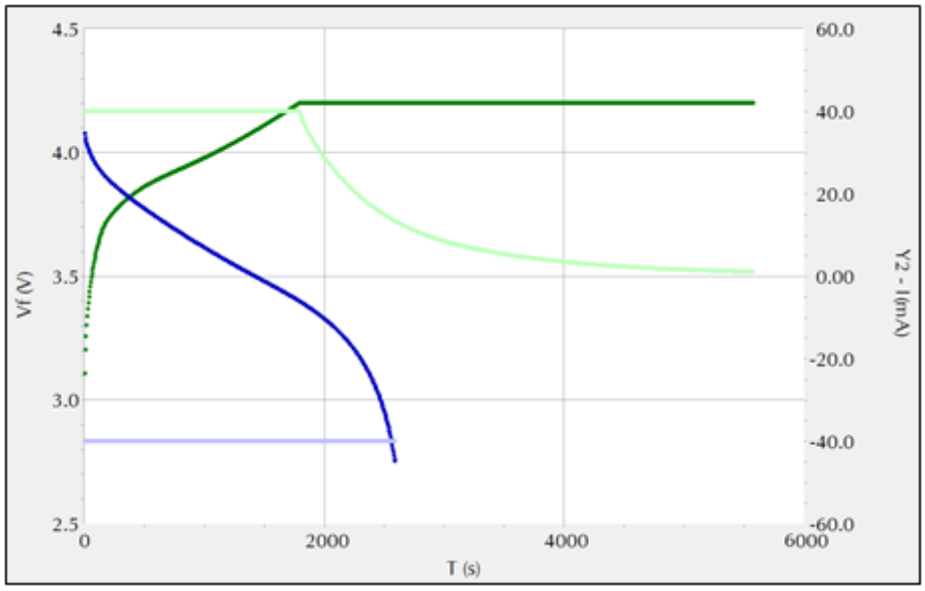

Figure 3.2. An example voltage and current vs time curve for a Lithium ion cell. Blue line represents discharge, while green line represents charge. [37]

Following this, separated the overpotentials as mentioned in for the lithium-ion batteries using the equation (3.2) given below [33]:

$$\tau_s = \frac{L^2}{D} \tag{3.2}$$

where, τ_s refers to the time scale, L is the characteristic length, D is the diffusion coefficient. This data has been adapted into this thesis to represent different regions of 30s pulse:

- The 0.5s instant represents the kinetics
- The 10s instant represents the electrolyte Lithium ion concentration gradient
- The 30s instant represents the Lithium solid state diffusion

As a conclusion, in this sub-section the overpotential phenomena was discussed followed by a study of the different types of resistances involved in the cell chemistry. Further, the cell polarization curves are studied to represent different time instants as different chemical phenomena.

Over the whole chapter, the different parameters relevant to the thesis work were studied with comprehensive literature review. The next section discusses the experimental setup, the different experiments done on the cells and the governing conditions.

4 Experiment

This chapter discusses the conditions and methods for the manufacture of the cells along with the cell testing. In the first part, the cell geometry, size and chemical composition of the cathodes and anodes are mentioned. The second part describes the test performed on the cells which are used in scope of this thesis work.

4.1 Cell chemistry

To have a common comparison standard between the cell packaging geometries, the chemistry for the anode, cathode, electrolyte and separator were chosen to be the same. All cells have been manufactured have the same material for the electrodes, i.e., $LiFePO_4$ as the cathode and graphite as the anode. Both the materials of the electrodes are from the same batch of raw materials for all the cells.

The separator used for the cell manufacture is a tri-layers Celgard 2325 grade. This type of tri-layered poly-olefin separator consists of 1 polyethylene (PE) layer sandwiched between two layers of polypropylene (PP), and is the most commonly used separator type. This is because of their chemical inertia and the safety feature the combination of PP-PE-PP offers. In the case of overheating, the PE layer melts, losing its porosity (i.e., mechanically blocking the Li^+ ion movement), while the PP layer prevents large dimensional changes until its own melting, thus preventing short-circuits.

The composition of the electrolyte solution strongly influences the temperature dependence of the capacity. This is related to the quality of the passivation of the graphite electrodes in the various solutions and to the transport properties of the passivating surface films that cover the graphite particles (discussion related to SEI layer formation). [38] For the cells manufactured by SPICY, the electrolyte solution used is a blend of ethylene carbonate (EC), propylene carbonate (PC) and di-methyl carbonate (DMC) in volume proportion 1:1:3, respectively, with 1M of LiPF6 and 2% weight of vinylene carbonate (VC). [39]

4.2 Cell geometry and size

The three packaging geometries (cylindrical, prismatic and pouch) were assembled in different ways, which are mentioned in the SPICY Deliverable 5.6 [39].

Jelly roll manufacturing was used to wind together the electrodes and separator in cylindrical and flat cores ***for cylindrical and prismatic cells***, respectively. While the cylindrical cores are basically rolls of electrodes with separators within them, for the prismatic cells, the cores resemble layers placed into a Z-shape. Next, the cells are welded together complete with the placing the current collectors and finally welding the top cap. The electrolyte is filled using different holders through the aperture at the top cap. It is necessary to ensure that the electrolyte solution covers every pore in the internal structure and the separator membrane. After this step, the cells are conditioned outside the dry room.

The ***pouch cells*** were manufactured separately. The process lacked a standardized equipment and therefore, needed a lot of workforce and manual job initially. In the first step, the electrodes and the separators were cut into layers using a cutting press and stacked into layers of 38 anodes, 76 separators and 37 cathodes. The terminals were drawn out and tabs were welded on them. The stacks thus formed were wrapped in two half-aluminium shells and heat sealed. The pouch cells were filled with the electrolyte solution in a glove box and the remaining side was welded. Then the cells were conditioned outside the dry room and the trapped gas bubbles in the structure were degassed as the last step. The three cell geometries manufactured are shown in Figure 4.1.

(a) (b)

Figure 4.1. Packaging geometries of the cells manufactured (a) Prismatic (L), Cylindrical (R), (b) Pouch [39]

The post manufacturing specifications of the cells are reported further in this subsection.The cell specifications of each geometry are mentioned in the Table 4.1.

	Cylindrical	Prismatic	Pouch
Lower Voltage limit (V)	2.5	2.5	2.5
Upper Voltage limit (V)	3.6	3.6	3.6
Maximum charge current (A)	50	4	50
Maximum discharge current (A)	100[1]	4***[2]	100[3]
Temperature operation range (°C)	[-10, +55][4]	[0, +45]	[-10, +55]**[5]

Table 4.1. Cell specification for cells of different geometries [39]

A weight analysis was done for all the cells and the average weight contribution of the different components of each cell are shown in Figure 4.2. A clear difference is noticed in the cells with soft packaging, i.e. the pouch cells, due to softer casing.

[1] for a 30s pulse

[2] normal cycling, rate tests upto 12A

[3] for a 30s pulse

[4] for charging [+5, +55]

[5] for charging [+5, +55]

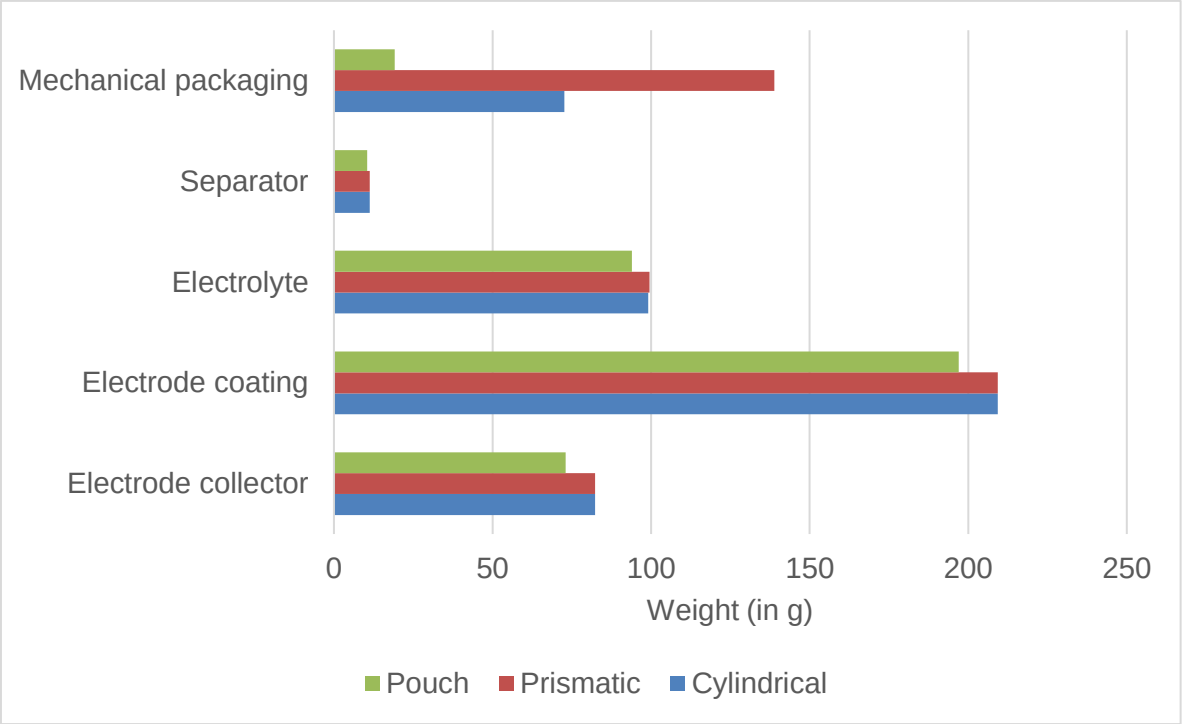

Figure 4.2. Weight analysis of the cells.

The weight results are documented as expected because of the hard cover being replaced by aluminum foil in the pouch cells, the packaging component and the overall cell weighs less. In the case of the prismatic cell, it requires more packaging than a cylindrical cell because of the higher surface area, as can be seen from the reception test data given in Table 4.2. The cells delivered were subjected to reception test and the data obtained are documented in the table:

	Cylindrical	Prismatic	Pouch
Energy density (Wh/kg)[6]	108.61	94.25	121.77
Capacity (Ah)	16.099	15.963	14.889
Weight (g)[7]	474.32	541.98	391.25
Height (mm)	125	125	-
Curved Surface area (mm^2)	19625[8]	31250[9]	-
Nominal voltage (V)	3.2	3.2	3.2[10]

Table 4.2. Cell geometry and reception test specifications

The data presented above were measured without any ageing. After that the cells were aged and cycled at different stages of State of Health (SOH). The following the section enumerates the different tests performed relevant to the current work.

4.3 Tests performed

Within the scope this thesis, only the life cycling tests have been included. It involves testing of the cells at different charging/discharging rates at different conditions of temperature over different states of health (SOH) or ageing time. In the cycle tests, the equivalent full cycles are observed over the ageing of the cells.

[6] Energy density, $E = \frac{Q \times V_{nom}}{m}$, where Q = Capacity, V_{nom} = nominal voltage, m = mass

[7] the weight differs from value in **Error! Reference source not found.** because the reception test results mentioned refer only to the cells chosen to be tested within the scope of this work.

[8] Curved surface area of cylindrical cell = $2\pi rh$

[9] Curved surface area of prismatic cell, considered to be cuboidal = $2(l + b)h$

[10] The nominal voltage for LFPC cells with the given chemistry is always 3.2V

In both calendar life and cycle life tests, two kinds of checks are given – short check-up (SCU) and extended check-up (ECU). The extended check-ups (ECUs) involve the measurements of capacity evolution, open circuit voltages (OCV) and internal resistances by pulse tests. Another test involves the temperature developed at the first ECU for different charging and discharging rates. Within the scope of this thesis, the capacity evolution, the internal resistance developed at different capacities (pulse tests) and the temperature are the most interesting.

The tests were carried out using the Extended Cell Test System (XCTS) provided by BaSyTec GmbH. According to the BaSyTec XCTS product brochure, it is a lithium ion cell formation and test system with up to 25A or 50A. It has the further advantage of low working expenses because of the option of energy recovery heat generation. Using the 50A system, currents up to 300A can be produced because of parallel operation facility. The system control is done using the high speed and precision BaSyTest software. Due to such features, this system finds application in test of large Lithium ion cells, high power tests, pulse tests and formation of lithium ion cells. [40]

The life-cycle test standards are documented in Spicy Deliverable 6.1. The usual test conditions as mentioned in this deliverable can be enumerated as follows [41]:

i. The state of charge calculated is the capacity calculated at usual discharge rate of 1C at 25°C.
ii. The state of health (SOH) refers only to the battery capacity decrease.
iii. The usual test conditions of C-rates for charging are 1C, 2C, whereas for discharging are 0.2C, 0.5C, 1C, 2C
iv. For this work, the SOC window for cycling is 0% to 100%
v. The end of life (EOL) is set to 80% of initial capacity and most test results in this work contains values for a minimum SOC around 80%.

The following sub-sections cover the tests performed on the cells which are relevant within the course of the work.

4.3.1 Capacity evolution of the cells

This test is perfomed to determine the cell deterioration or capacity loss. Of special interest is the capacity deterioration over the possible number of equivalent full cycles (EFC). The capacity deterioration is measured as SOH drop.

As mentioned earlier in the discussion of the test conditions, the state of health (SOH) refers only to the battery capacity decrease. The SOH is not a well-defined physical quantity. It can

be defined and determined by using any measurable quantity that changes with ageing of the cell for example capacity, internal resistance, cell impedance, cycling temperature gradient changes etc., and is monitored with respect to the values for a new cell. Therefore, such details are not provided by the manufacturers and have to be independently determined by the testing infrastructure. There is no precise definition of SOH agreed upon uniformly by industries or scientists [42]. The SOH estimation within this work, as mentioned, has been done by measuring changes in the capacity of a fully charged cell. It can be depicted using the equation (4.1) [42]:

$$SOH = 1 - \frac{Q_{full,aged}}{Q_{full,new}} \tag{4.1}$$

Here, $Q_{full,aged}$ refers to the capacity of the aged (current state) battery at full charge (that is an SOC of 100%), while, $Q_{full,new}$ refers to the capacity of a new unaged battery at 100% SOC. There are many different methods to calculate the capacity of the cell, for e.g. coulomb counting and open circuit voltage method [42]. But discussions of these methods are beyond the scope of this work.

For this work, the method for the capacity evolution and the subsequent SOH calculation is described below with the help of Figure 4.3. The figure shows a sample plot taken from a cylindrical cylinder testing. It helps to show how the SOH is being calculated. The cells were charged and discharged using the conventional constant current – constant voltage (CC+CV) and constant voltage (CV) protocols. [43] The CC+CV protocol is the most popular charging protocol which involves a low rate constant current charging to a predefined cut-off voltage followed by float charging at the cut-off voltage until the current drops to very low preset value. The positive current and instantaneous capacities are for charging, while the negative values depict discharging.

i. An un-aged cell is discharged completely and the residual capacity is measured and noted.
ii. Next the cell is charged again first with constant current (CC) and then with constant current + constant voltage (CC+CV). When the cell is fully charged, the capacity is measured again and noted.
iii. This fully charged cell is discharged again and another discharge cycle, as described in step ii above, is carried out.

iv. The cell is again charged again and the cell capacity after the second discharge is noted, as saved as the $Cap_{reference}$ (reference initial capacity) of the unaged cell. This corresponds to the capacity at 100% SOH.

v. Steps i through iv are repeated for the aged cell and the cell capacity after the second discharging-charging step is noted and saved as $Cap_{i,aged}$ (the capacity of the aged cell at the i[th] step). The SOH of the aged cell is calculated using the equation

vi. (4.2):

$$SOH_i = \frac{Cap_{i,aged}}{Cap_{reference}} \times 100 \quad (4.2)$$

where, SOH_i is the state of health at the i[th] step

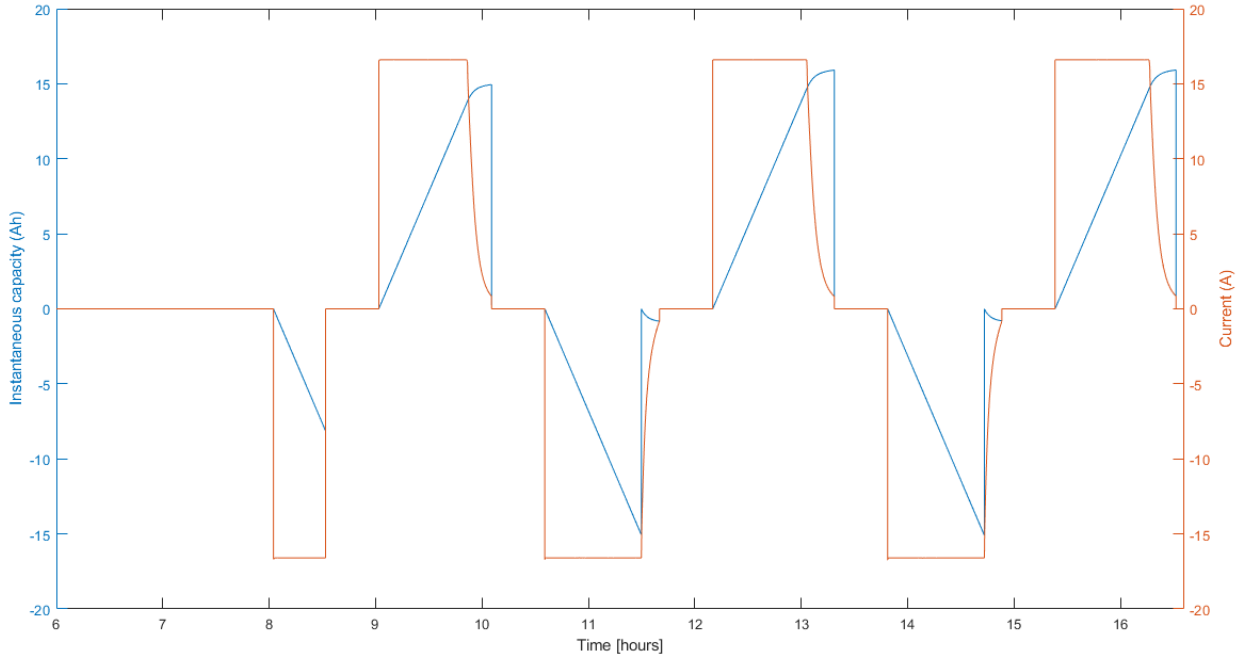

Figure 4.3. A sample plot to show the capacity evolution for the calculation of SOH

An aged cell has reduced full capacity and the number of full cycles it has gone through its life is not a linear curve with linear multiplicity. This quantity is defined by the term equivalent full cycles (EFC). The EFC can be calculated using the equation

(4.3) [44]:

$$N_{eq} = \frac{W_{tot}}{2 \times U_{nom} \times Q_{init}} \quad (4.3)$$

Here, N_{eq} = equivalent full cycles, W_{tot} = accumulated energy throughput for the cycled cell, U_{nom} = specified nominal battery voltage, Q_{init} = measured initial battery capacity

The capacity evolution or deterioration is studied with respect to changes in SOH and equivalent cull cycles (EFC). These conditions are checked for the cells of the three geometries for different conditions of temperature and cycling current rates. These results are discussed in the next chapter.

4.3.2 Temperature developed over cycling

To determine the temperature gradient over the three geometries at similar conditions, the temperatures were measured for the first extended check-up (ECU) cycle with different cycling current rates. In all the cases though, the charging was done with a rate 1C, but the discharging was tested with slow to fast cycling.

The temperature sensors used for the tests were the Negative Temperature Coefficient (NTC) sensors. This is the most commonly used type of temperature sensors, and in this case, the temperature shows an inverse relation with respect to the resistance. [45] NTC thermistors are high precision and can give a resolution and accuracy as low as 5mK.[11]

The different stages of the charging and discharging were identified by using the data for the cell voltage during the same stages.

The method used for the automated calculation of the SOC is the coulomb counting method. The Coulomb counting method measures the discharging current of a battery and integrates the discharging current over time in order to estimate SOC. Coulomb counting method is

[11] The temperature sensor data has the potential to be improved by using embedded temperature sensors in the case of pouch cells or temperature sensors in the jelly roll structure of the prismatic and cylindrical cells

done to estimate the SOC_t, which is estimated from the discharging current, $I(t)$, and previously estimated SOC values, SOC_0. SOC is calculated by the equation (4.4) [46]:

$$SOC_t = SOC_0 - \frac{\int_0^t I(t)dt}{Q_n} \tag{4.4}$$

where, Q_n is the nominal capacity measured in the beginning of cycling, and t is the time at which the SOC needs to be calculated..

4.3.3 30s pulse test

In this work, the internal resistance has been calculated for 30s charge and discharge pulses at the 0.5s, 10s and 30s time-instants. This section discusses the experimental procedure for the same.

Two types of pulses are used during the test: one for increasing the SOC and another 30s pulse for measuring the internal resistance,While charging, first the SOC is determined for a fully discharged cell and a pulse of 1C is applied for 30s at that SOC. Next, the cell stabilizes for a while without a pulse and then it is charged again at 1C this time to increase its SOC. In the case of discharging, the only difference is that a current is drawn from the cell. This is explained using **Error! Reference source not found.** and **Error! Reference source not found.**.

This method is used for the SOCs: 5%, 10%, 20%, 30%, 40%, 50%, 60%, 70%, 80, 90% and 95%. Further, for each 30s pulse, the internal resistance is calculated at the 0.5s, the 10s and 30s instant. This is done by calculating the instantaneous change of voltage in and dividing it by the current at that time in Figure 4.4(which is approximately equal to 1C), as shown in the equation (4.5):

$$IR = \frac{\frac{\partial V}{\partial t}}{I} dt \tag{4.5}$$

Where, ∂V refers to the infinitesimal change in voltage over ∂t in Figure 4.4 and I refers to the current at the stage (which is usually constant at 1C or 16A)

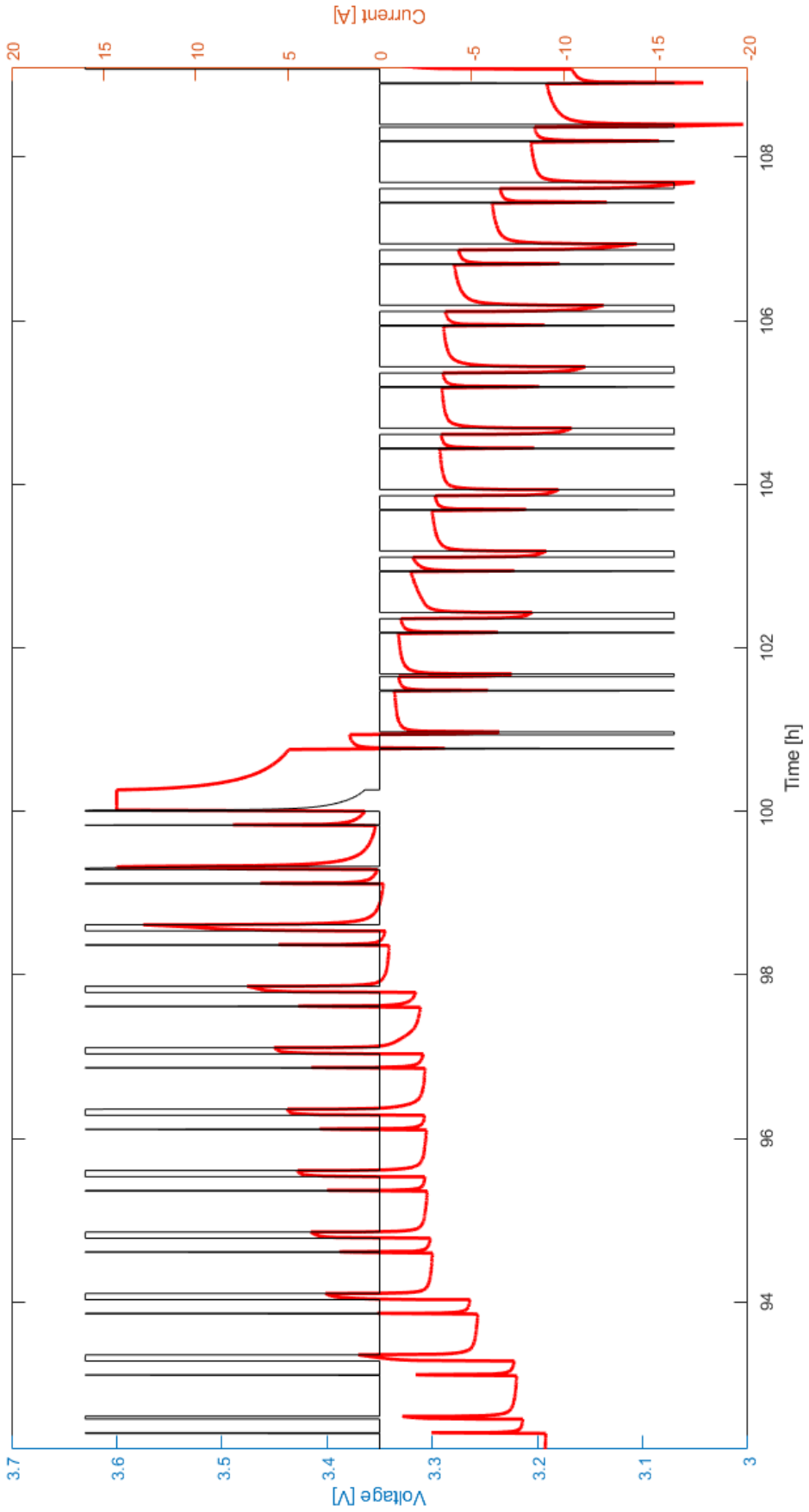

Figure 4.4. Explanation for a 30s pulse test with current pulses and voltage evolution

5 Discussion

MATLAB Data Processing and Visualization was used to extract, sort, edit and visualize the experimental data for ease of analysis. It was found that the data for cells under the same conditions of cycling rate and temperature show similar results and therefore the cell data were averaged. Further, in certain cases, data interpolation and extrapolation to maintain uniformity. The following sub-sections would discuss the experiment results from the previous chapter along with any assumptions made in each case.

An initial discussion of the cell chemistry and materials) shows the measured values for parameters like cell weights, capacity and energy densities. It was already discussed a possible reason for the lower weight of the pouch cells due to its light-weight aluminum pouch cover and lack of any hard covering. A weight analysis of the different components of the cells is also done in **Error! Reference source not found.**. The difference in the weights of the prismatic (heavier) and cylindrical cells can be explained using the higher surface area of cover for the case of the prismatic cells leading to higher requirement of metallic cover material. The added weight is the case of the prismatic cells can also be attributed to an added metallic/steel support for stability. [21] A further reason could be that in a pouch cell, the cathode, separators and anode are stacked instead of wound, as can be seen in Figure 2.2. This approach increases packaging density to the maximum and saves weight, thus increasing energy density of the cell. The packaging density when grouping cylindrical cells is low due to their round shape, and the cell case is comparatively heavy. [21]

Due to the weight comparisons as discussed, it is not surprising that energy density (Wh/kg) of pouch cells is the highest followed by cylindrical cells followed by prismatic cells. (Considering that all the cells have a capacity close to 16Ah and a nominal voltage has been assumed to be the same at 3.2V).

While all the cells have been manufactured to be around 16Ah, Table 4.2 shows a minor difference in the capacities of the cells. While cylindrical and prismatic cells are almost equal to 16Ah (cylindrical slightly higher), the capacity of pouch cell is a little less than 15Ah. A look at the **Error! Reference source not found.** can provide a possible reason for it. It shows that weight of electrode collector + electrode coating + electrolyte material is clearly less in the case of pouch cells as compared to prismatic and cylindrical geometries. The less electrode + electrolyte content in pouch cells might explain the reduced capacity.

The next sections discuss first the performance of a new unaged cell with respect to internal resistance profiles from pulse test and then the temperature evolution over cycling of each

geometry. The section after that discusses the effect of ageing on the cells, namely, the capacity deterioration and equivalent full cycles at different conditions of temperature and cycling, and the influence of ageing on internal resistances. For ease of study and data representation, all the data values for the same geometry and same test conditions are averaged out.

5.1 Performance of unaged cells

The data obtained from the tests are then pre-processed by averaging the values for the same geometry and same test conditions (C-rate and temperature). Also, for simplicity, only the data for 0.3C-rate condition are considered.

5.1.1 Internal resistance at 100% SOH for different cell geometries

The unaged cells are subjected to the 30s pulse test as explained in the previous chapter. This internal resistance data was calculated over different State of Charge (SOC) of the cycling process, to represent the pulse polarization curve at every SOC considered. The resulting data comparison between the different cell geometries at the same conditions is represented in **Error! Reference source not found.** and **Figure 5.2**.

It can be seen from the figures that the internal resistance values for cylindrical and prismatic geometries are almost identical in most cases, though the values for pouch cells are much lower. It is interesting to note that there is a sharp drop in internal resistance value at the start of the charging pulse (around 0-10% SOC). A similar phenomenon is observed for pouch cells in the reverse direction in the case of the discharge pulse. While in most cases, the internal resistance values of prismatic and cylindrical are higher than pouch, at the end of the discharge cycle, there is a sharp increase in the internal resistance curve for the pouch cell to reach values quite higher than prismatic and cylinder.

It is also notable from **Error! Reference source not found.** (charging pulse at 0.3C and 5°C) that there is a characteristic decrease in the value of internal resistance when approaching an SOC of 70% in all geometries at the instants 10s and 30s (though it is negligible at 0.5s). Similarly, from **Figure 5.2** (discharging pulse at 0.3C and 5°C), during the discharge process, there is sudden peak of internal resistance around the 70% SOC mark for all geometries.

It can be easily concluded from the figures that in general the internal resistances of cylindrical and prismatic cells are higher as expected, at very low SOC values, this parameter value is higher for the pouch cells. Since development of internal resistances is directly related to capacity losses, cylindrical and prismatic cells have higher capacity losses in general. But if pouch cells are used at a lower SOC for longer period of times, this might lead to steeper capacity losses for it.

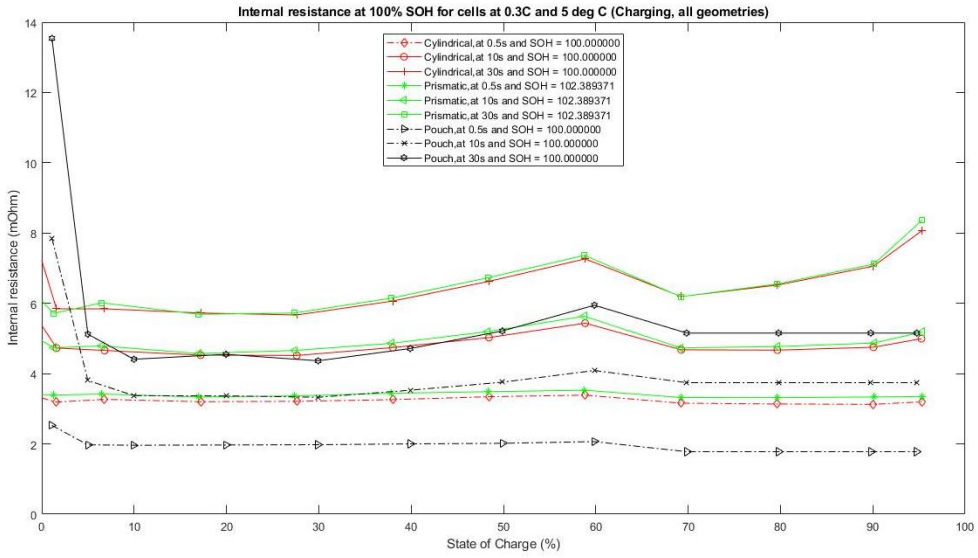

Figure 5.1. Internal resistance comparison for a charging pulse

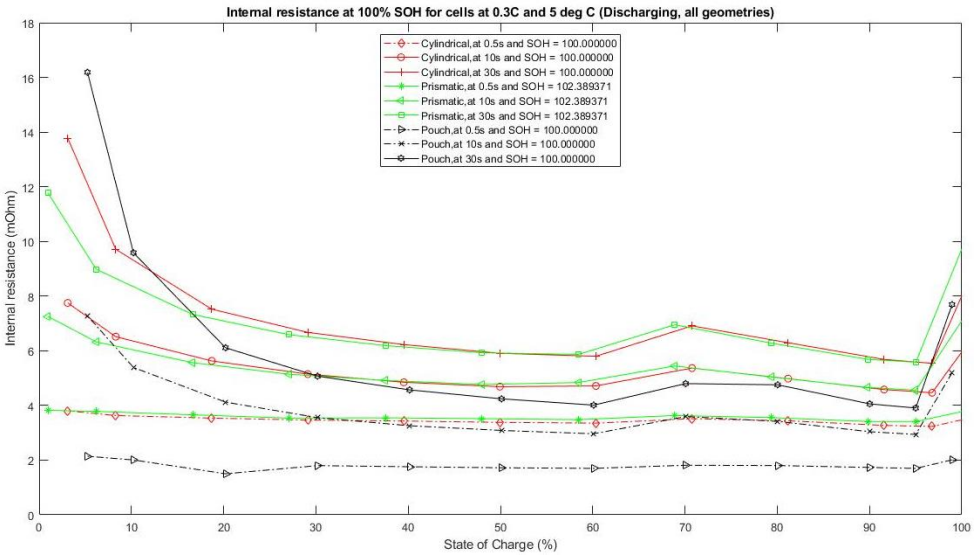

Figure 5.2. Internal resistance comparison for discharging pulse

Error! Reference source not found. below enumerates the values of internal resistance at the SOC values of 5%, 50% and 95%. Neglecting the sudden surges in internal resistance in pouch cells around the early SOC regions, the internal resistance follows the general trend of: prismatic >= cylindrical > pouch.

Geometry	**5% (in mOhm)**			**50% (in mOhm)**			**95% (in mOhm)**		
Pulse instant	*0.5s*	*10s*	*30s*	*0.5s*	*10s*	*30s*	*0.5s*	*10s*	*30s*
Charging pulse for cells at 5°C/0.3C									
Cylindrical	3.241	4.682	5.845	3.343	5.026	6.626	3.196	4.995	8.059
Prismatic	3.411	4.773	5.929	3.486	5.197	6.727	3.349	5.183	8.367
Pouch	1.972	3.806	5.122	2.017	3.756	5.214	1.779	3.743	5.155
Discharging pulse for cells at 5°C/0.3C									
Cylindrical	3.741	7.299	12.29	3.381	4.686	5.909	3.225	4.455	5.530
Prismatic	3.792	6.538	9.616	3.516	4.764	5.927	3.411	4.558	5.582
Pouch	2.142	7.278	16.19	1.72	3.085	4.242	1.697	2.940	3.906

Table 5.1. Internal resistance at selected SOCs for a charging pulse

5.1.2 Temperature developed over cycling

One of the major safety issues in commercial Lithium ion batteries especially in EV and HEV is associated with the temperature developed over the cycling period. Therefore, it becomes an important parameter for cell performance evaluation. Data for temperature developed is processed from the first ECU of unaged cells. For uniformity, the temperature profiles were plotted for cells stored at 0.3C and 5°C. During the cycling, the charging was done at 1C, but the discharge was done at 0.2C, 0.5C, 1C and 2C. **Figure 5.3** shows the temperature evolved over the cycles for the three geometries, along with the voltage of the cells to represent the cyclies.

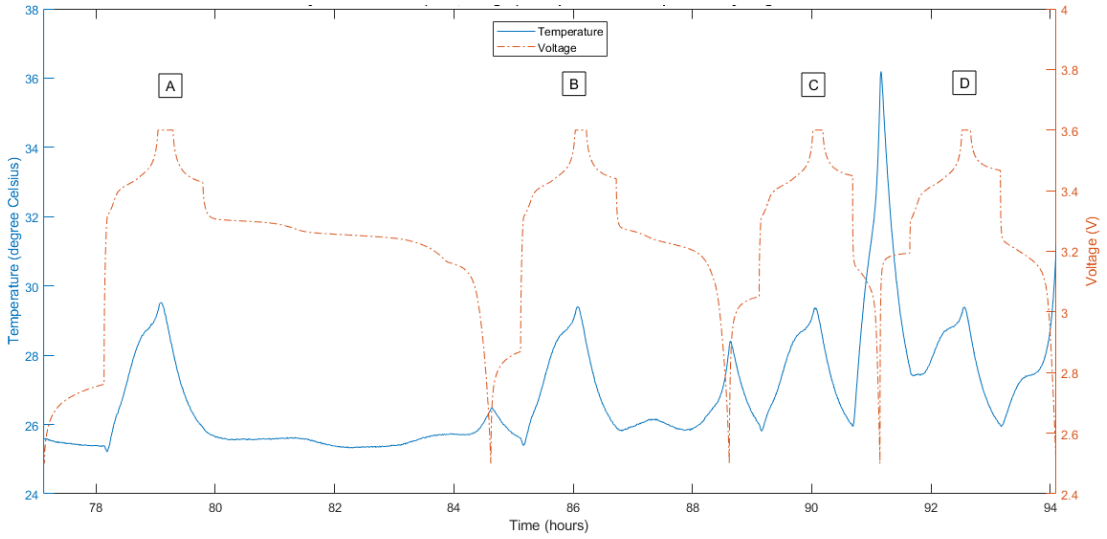

(a)

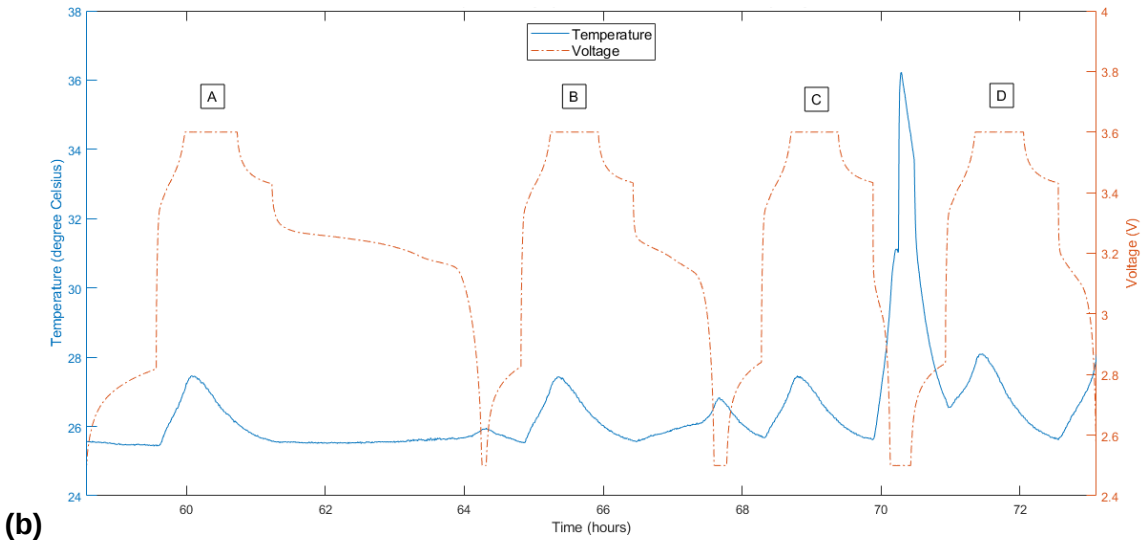

(b)

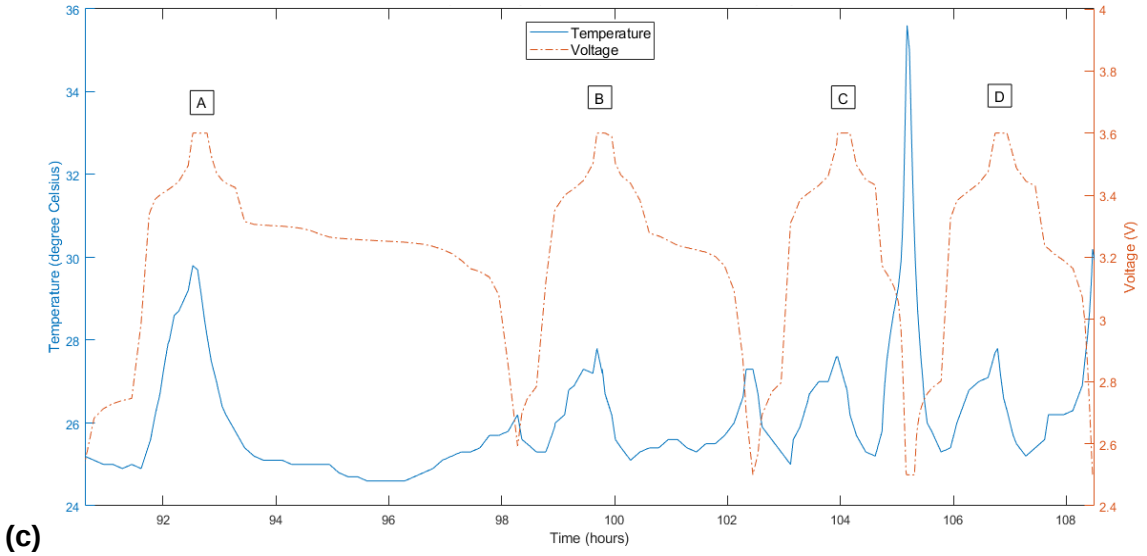

(c)

Figure 5.3. Temperature developed over cycling for (a) Cylindrical, (b) Prismatic, (c) Pouch cells

The labels in the figure refer to one cycle each and are characterised by the C-rates as shown in Table 5.2.

Label	**A**	**B**	**C**	**D**
Charging	1C	1C	1C	1C
Discharging	0.2C	0.5C	2C	1C

Table 5.2. Table showing the cycle characteristic denoted by labels in Figure 5.3

The temperature profile shows a common trend among all the geometries. There are two local peaks for each cycle, one at the end of the charging cycle and one at the end of the discharging cycle. The temperature at the end of the charging cycle (at the rate of 1C) remains almost same at the end of all the charging cycles, except for the first charging cycle of pouch cell where it is slightly higher than the subsequent cycles. Table 5.3 shows the temperature gradient developed between the beginning of the charging cycle and the peak temperatures.

Cell Type	**First 1C Charge (°C or K)**	**1C discharge (°C or K)**	**2C discharge (°C or K)**
Cylindrical	4.14	1.83	10.19
Prismatic	2	1.34	10.51
Pouch	4.8	2.5	10.30

Table 5.3. Temperature gradient developed at different charge/discharge cycles

The first column in the table shows the temperature gradient during the charging cycle at 1C (the local peak) with respect to the temperature at the beginning of the cycle, while the next two columns show the gradient at the end of 1C and 2C discharge with respect to the temperature at the start of the cycle.

A significant observation is the global peak in temperature developed at the end of the 1C charge - 2C discharge cyce for all geometries. **Error! Reference source not found.** below shows a a zoomed in section for this cycle on the same scaled axis. For each cell, the intitial temperature at the start of the whole cycle, the temperature peak at the end of the first charging cycle and temperature peak at the end of discharge cycle are also mentioned. Please note that the difference in time scale is not a significant factor as all data is for the first ECU of all geometries.

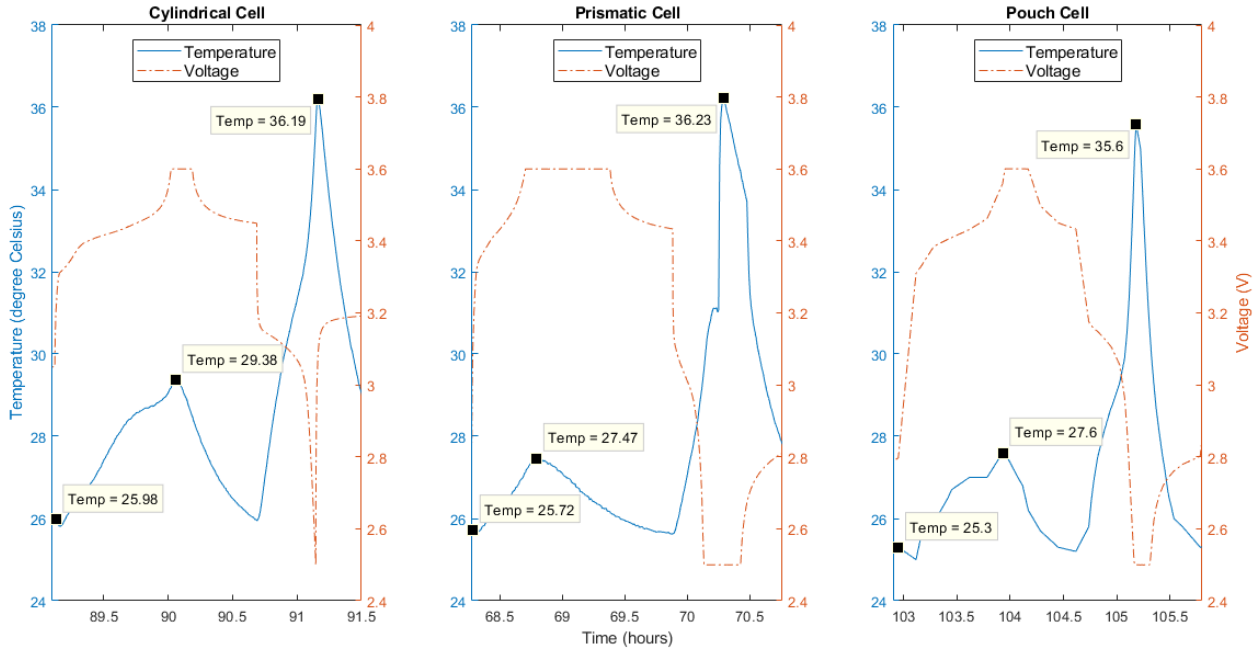

Figure 5.4. Temperature profile for 1C charge and 2C discharge for all three geometries**.**

The local peak temperature at the end of the charging for the case of the cylindrical cell is higher than the other two geometries. But, the maximum temperature developed in each case remains the most important parameter for this study. For the 1C charge-2C discharge case, while the temperature gradients are almost similar, the absolute temperature at the end of the 2C discharge is slightly lower for the pouch cell.

This is a reasonable conclusion since the problems with thermal management and a lack of proper passage for waste heat in prismatic cells are well known. This mostly because of the higher mechanical stresses. [21] This leads to the temperatures building inside especially

when subjected to rapid discharging currents. A cylindrical cell has the least surface area for heat dissipation [47] , which explains the higher temperatures developed in it. As discussed earlier, pouch cells usually use thin slices of electrodes and separators which are stacked in layers. Thin electrodes can enhance the fluency of ion diffusion and improve the electrochemical reactions which helps high rate discharges and long term performances due to the mild temperature variation [47], which might also indicate the lower temperature developed in pouch cells and no rapid increase in temperature at 2C.

Summarizing the temperature profile results, it is observed that the peak temperatures are generated at the end of charging or at the end of discharging, while higher temperatures are reached for higher C-rates. This is because over both charge and discharge, the Li ion migrate inside the cells to establish a concentration gradient, which generates heat as a function of applied current [48]. These temperatures are higher at the end of the discharge, which increases with increase in discharge C-rate from 0.2C to 2C. It is expected that the temperature rise will be even higher at higher C-rates.

Better results can be expected by testing at discharge rates higher than 2C. Further a more comprehensive study can be done with monitoring the internal temperatures developed in the cells by using methods such as using embedded temperature sensors in the case of pouch cells or temperature sensors in the jelly roll structure of the prismatic and cylindrical cells.

[INCLUDE A CONCLUSION OF PERFORMANCE ANALYSIS OF THE CELL]

5.2 Ageing effects on cells of different geometries

The previous section discusses the performance of unaged cell. This section discusses the behavior of the cells during aging at the given temperature and C-rates. First, the capacity deterioration is discussed with respect to the equivalent full cycles (EFC). The next subsection discusses the effect of aging on the 30s pulse test results for the selected conditions of temperature and C-rates.

5.2.1 Ageing characteristics over equivalent full cycle (EFC)

The concept of equivalent full cycles (EFC) has already been discussed in the previous chapter. Because of ageing, the way one whole full cycle is defined differs from one time-step to other. The capacity itself undergoes changes because of the cyclic and storage

deterioration. Different cell chemistries therefore show different drop in capacities and different number of equivalent cycles possible over that the ageing period. Figure 5.5 shows the equivalent number of cycles for each geometry of cell for different cell conditions over the ageing period as shown by the State of Health (SOH). As discussed already, the SOH has been determined by drop of capacity of the cells, therefore SOH is used as the parameter to describe the ageing process.

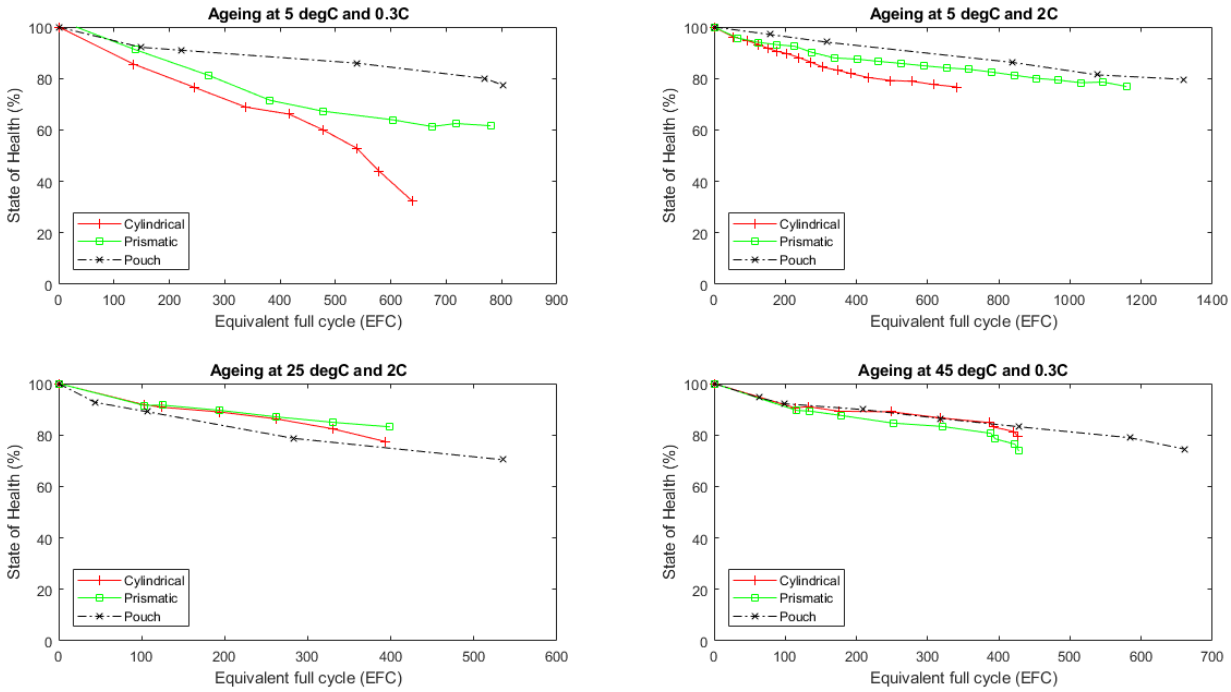

Figure 5.5. Capacity deterioration and the number of equivalent cycles obtained over the ageing period for different cycling conditions.

As already discussed in the earlier chapters that the charging/discharging protocol used in these experiments, namely the constant current-constant voltage (CC+CV) and constant voltage (CV) protocols, leads to a rapid deterioration of cell capacity as compared to other charging protocols. But all the cells are expected to have had the same effect on their ageing because of that. Another major influencing factor on the capacity fade is the depth of discharge (DOD), but it has not been considered here as all the cells are cycled between 0% and 100% SOC.

In electrochemical terms, the major cause of ageing is because of the degradation of electrodes. [25] The ageing phenomenon is graphite anode based Lithium ion cells is associated with the formation of a solid electrolyte interface (SEI) layer formation. The SEI layer is formed from the lithium inventory of cathode and electrolyte salt. It is vital to the performance of the lithium ion cell, since the entirety of the anode must have a uniform layer of SEI to prevent further disintegration of the electrolyte. Therefore, the initial cycles of

lithium ion cell operation show a considerable drop in capacity due to the irreversible SEI layer formation out of the lithium inventory. [49] This is observed as an initial high rate of loss of capacity followed by reduced loss rate in Figure 5.5.

An optimized SEI layer is expected to have negligible electrical conductivity, high electrolyte diffusion resistance while having high lithium selectivity and permeability. Once it is properly formed, further decomposition reactions with salts and solvents are prevented as electrons cannot transfer to or through the layers. Properties of an ideal SEI formation are high electrical resistance, high lithium selectivity, high strength, tolerance to expansion and contraction stresses. [49]

In real cases, the SEI-layer thickens by repeated cycling gradually due to electron exposure to electrolyte and electrolyte diffusion to graphite surface. This not only leads to electrolyte decomposition but also might lead to loss of active lithium. [49] The four different ageing mechanisms attempt to explain various ways in which this can happen. Therefore, this study primarily analyses the ageing phenomenon with respect to the SEI layer formation and the related four ageing mechanisms. [25] It must also be noted that most studies agree to deal with the cycle number as the main time notion, and therefore, the ageing curves here are plotted against the equivalent full cycle. While in practice higher C-rates should accelerate the ageing of the cells, but in practice, the relation between C-rates and the capacity fade is found to be complex. [25]; [26] Even so, the highest C-rate in this study (2C) does not have significant effect on the ageing mechanism. Ageing and SEI layer formation strongly depend on the cycling temperature. There is an optimum temperature (usually moderate temperatures) for cycling which may be different for each cell. Temperatures above this favors further SEI layer formation and thus, accelerates ageing. [50]

A first look at the ageing curves in Figure 5.5 show a low capacity degradation in the case of pouch cells as compared to other geometries in all but one operating conditions. To analyze more thoroughly, the capacity drop can be observed after a fixed number of equivalent cycles in the case of all the geometries under all operating conditions. Such an analysis is shown in Table 5.4 below.

Cycling conditions	**Remaining capacity in terms of SOH after 400 EFCs (%)**		
	Cylindrical	**Prismatic**	**Pouch**
5°C, 0.3C	66.69	70.70	88.13
5°C, 2C	81.40	87.49	92.84

25°C, 2C	76.94	83.12	74.82
45°C, 0.3C	82.63	78.10	84.02

Table 5.4. Table showing the remaining capacities of cells, in terms of SOH, after 400 cycles (EFC)

In cylindrical cells, the capacity fade at 5°C and 0.3C is the lowest. But any increase in either the C-rate or the temperature leads to a slower capacity fade. This directly indicates the influence of the ageing mechanism related to Li plating. Low temperatures affect the anode kinetics and results in the reduction of the solid state ionic diffusion rate, which increases the risk of Li plating. At higher C-rates or temperatures, the anode kinetics improve and thus resulting in reduced cell degradation rate, with higher temperatures being more suitable for maintaining a higher capacity. [24] Further the higher degradation rate for the case of the cell at 25°C, 2C is attributed to the combined effect of higher temperature developed due to the cycling temperature and higher cycling rate (it was observed in a previous section that temperature developed in cylindrical cells at 2C charge rate is the highest). Higher temperatures developed due to the combined factors can damage the morphology of the SEI layer leading to decomposition of the electrolyte. A further ageing mechanism can be particularly seen in the case of cylindrical cell at 5°C and 0.3C, which is the loss of active material (LAM), characterized by the abrupt capacity losses during the latter stages of ageing, which indicates structural degradation of electrodes at this stage. [24] Minor evidence of LAM is also seen at the end of the curve at 45°C and 0.3C.

For the case of prismatic cells, the trend resembles cylindrical cells, but with a lower rate of capacity deterioration. This might be because of Li plating but at a lower degree. Further, no evidence of hidden capacity loss due to LAM is seen in this case, except for a minor evidence of it at 45°C and 0.3C resembling the cylindrical cells at the same condition. This follows expectations as loss of active lithium (or LAM) is rather higher at elevated temperatures.

The pouch cells have the best capacity retention out of all the geometries under most cycling conditions (except one anomalous condition of 25°C and 2C). Since all the graphite anode based Lithium ion cells show initial ageing due to the formation of SEI layers on the electrode, it can be inferred that the effect of SEI layer in the case of pouch cells not only has the minimum surface area but is also the most uniform and most stable. [24]; [25]; [49] This might be because of the less mechanical and thermal stresses in the geometry of pouch cells due to the stacked structure and soft casing. This can potentially be a significant advantage of pouch cells compared to cylindrical and prismatic geometries, with respect to

SEI layer formation. This is inferred because the only factor determining the ideal SEI layer not common to all the geometries is the tolerance to expansion and contraction stresses (mechanical stresses).

The pouch cells also undergo improved capacity retention moving from 5°C, 0.3C to 5°C, 2C, resembling both cylindrical and prismatic geometries, suggesting a small Li plating induced LLI process because of reduced kinetics at low temperatures and low C-rate. Overall, pouch cells show a much better performance at lower temperatures. But the effect of high temperature induced SEI layer formation (temperature increase from 5°C to 45°C) overcompensates any improvement in improvement of kinetics and results in faster capacity fade at higher temperatures. It must be noted that the behavior of pouch cells at 25°C and 2C is anomalous and cannot be explained suitably with the literature studied.

Summarizing the results, it is observed that the pouch cells have the best overall capacity retention among all structures and is particularly favorable towards formation of an ideal SEI layer. Further, it is observed that all the geometries undergo Li plating at low temperatures of operation. A comparison of the high temperature capacity fading suggests that the optimum temperature of cycling is highest for cylindrical cells followed by prismatic cells with pouch cells having the least. Both the prismatic and cylindrical geometries show tendencies of loss of active material (LAM) with an abrupt increased capacity fade, with cylindrical cell at 5°C and 0.3C showing a significant drop. Any instances of LAM suggests a possible electrode deterioration.

5.2.2 Change in internal resistance by ageing (during a charging/discharging pulse)

Ageing leads to an increase in internal resistance and higher the resistance increase higher is the capacity loss of the cell/ Therefore, it is more interesting to note the incremental change in internal resistance over ageing period on the different cell geometries. This section analyzed the incremental change in internal resistance during charging and discharging. The plots with the absolute values of internal resistances can be found in

Figure 5.6, Figure 5.7 and Figure 5.8 show the incremental change in internal resistance of a cell during a 30s charging pulse at different instants of 0.5s, 10s and 30s, compared over different geometries stored at different temperatures. The incremental change is calculated by taking the ratio of the internal resistance of the cell at an aged stage with respect to the internal resistance at 100% State of Health (SOH) or unaged stage.

A very first observation shows that a pouch cell at elevated temperatures (45°C) shows a positive change, that is a reduction in the internal resistance value (ratio less than 1) at all time instants of measurement. Whereas a prismatic cell at the same temperature shows the highest increase in internal resistance value at almost all measurement, though the difference is negligible compared to the other geometries. Table 5.5 shows that the increment is highest for the prismatic cell stored at 45°C with a value of 1.394, while the pouch cell at 45°C shows a maximum decrease of almost by half.

However, on comparing the absolute values, it can also be seen that the internal resistance values for pouch cells under most conditions are the least.

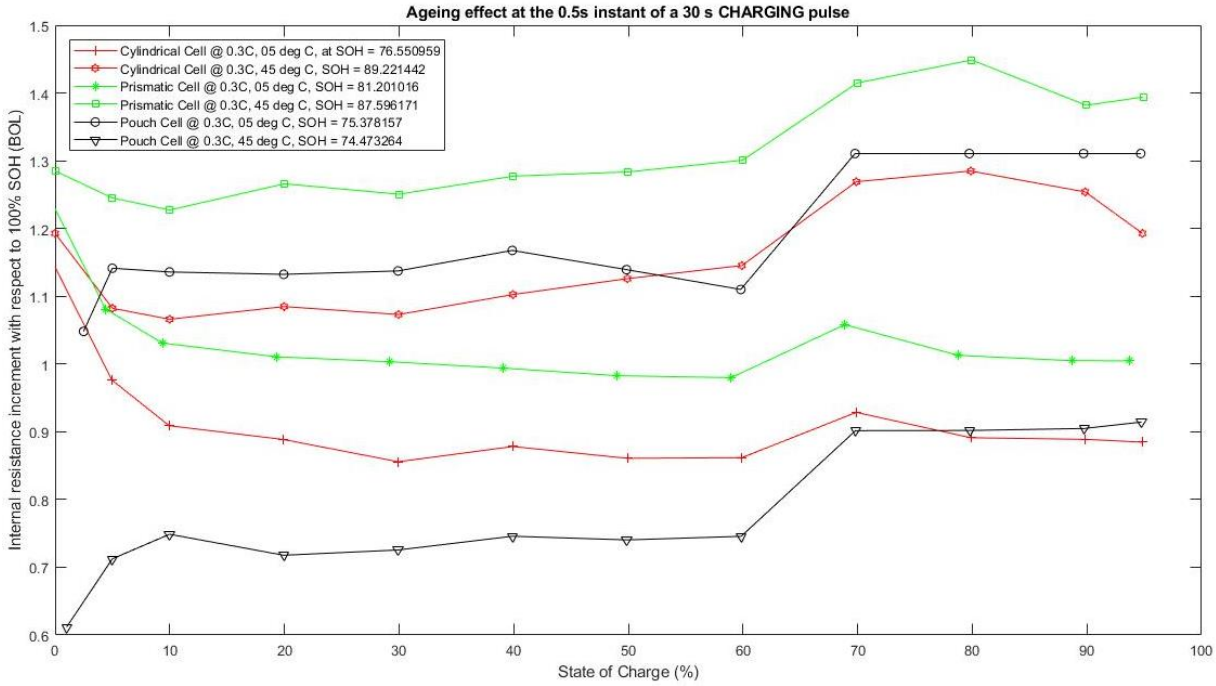

Figure 5.6. Incremental internal resistance (compared to 100% SOH) at the 0.5s instant of a 30s charging pulse

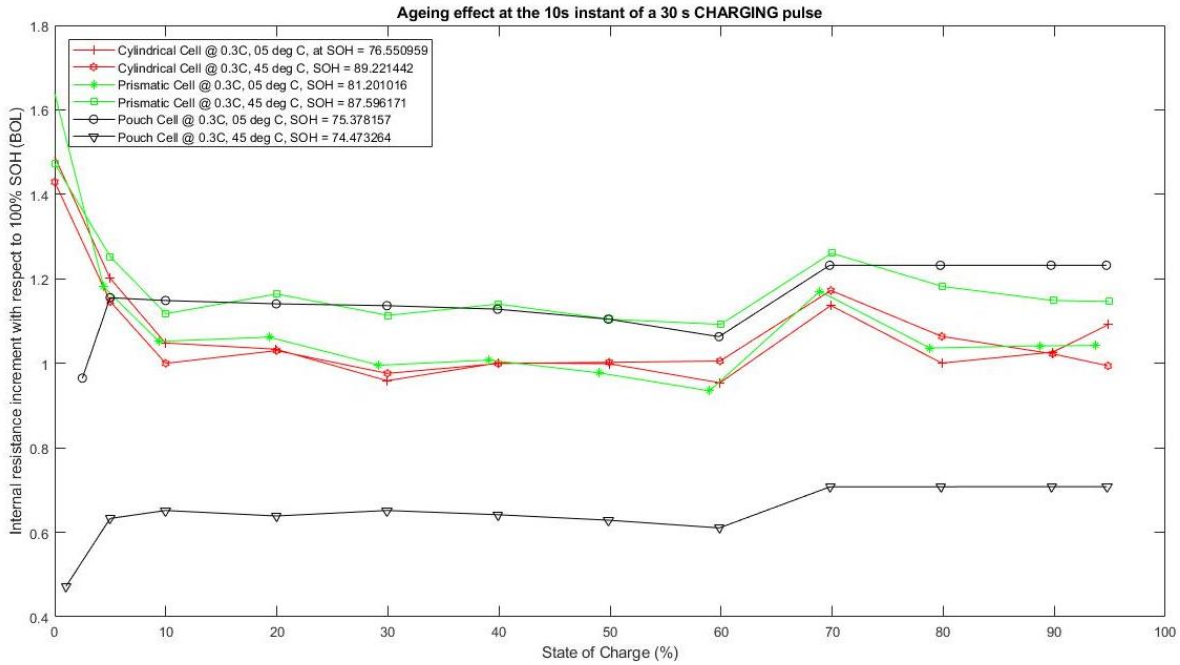

Figure 5.7. Incremental internal resistance (compared to 100% SOH) at the 10s instant of a 30s charging pulse.

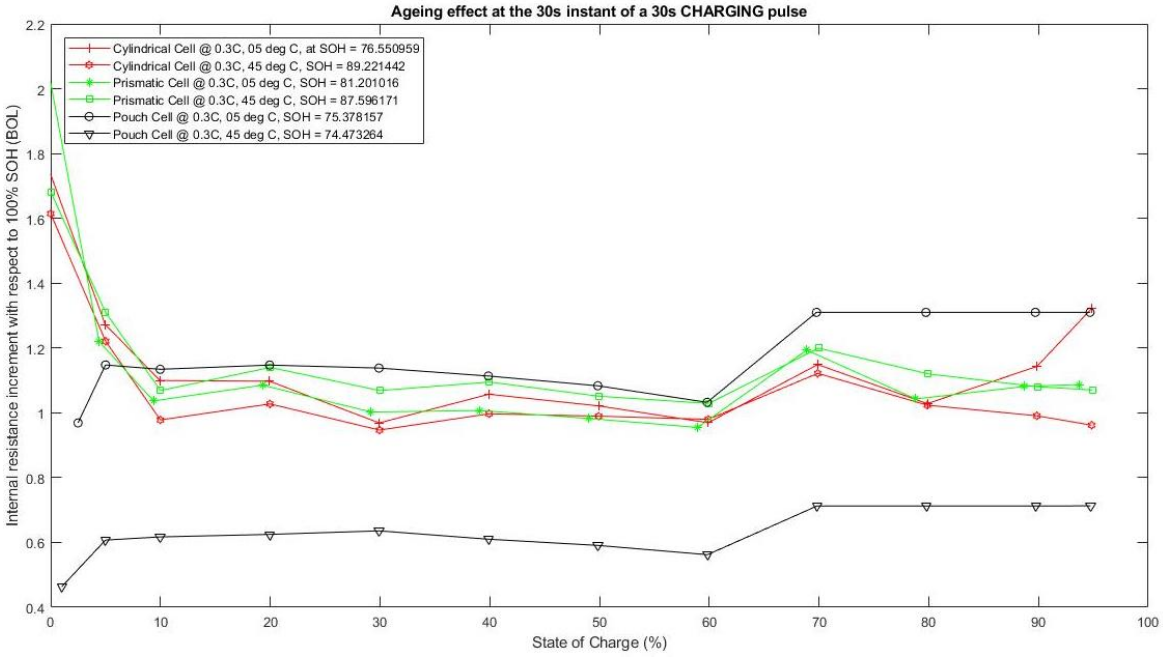

Figure 5.8. Incremental internal resistance (compared to 100% SOH) at the 30s instant of a 30s charging pulse.

Figure 5.9, Figure 5.10 and Figure 5.11 show the incremental change in internal resistance of a cell during a 30s discharging pulse at different instants of 0.5s, 10s and 30s, compared over different geometries stored at different temperatures.

For the discharge pulses, the internal resistances increase by less magnitude than in the case of charging pulse (max increase is 1.222) but the pouch cell at elevated temperatures shows a peculiar trend under a discharge pulse. At 45°C, the internal resistance value in the case of pouch cells shows a constant decrease as compared to the case at 100% SOH with a value up to almost 40% of the unaged cells. This can perhaps be explained by the results from the last section where the ageing of the pouch cells did not suffer by an increase in temperature or increase in C-rate. Therefore it brings a further stability to the functioning of the pouch type cells.

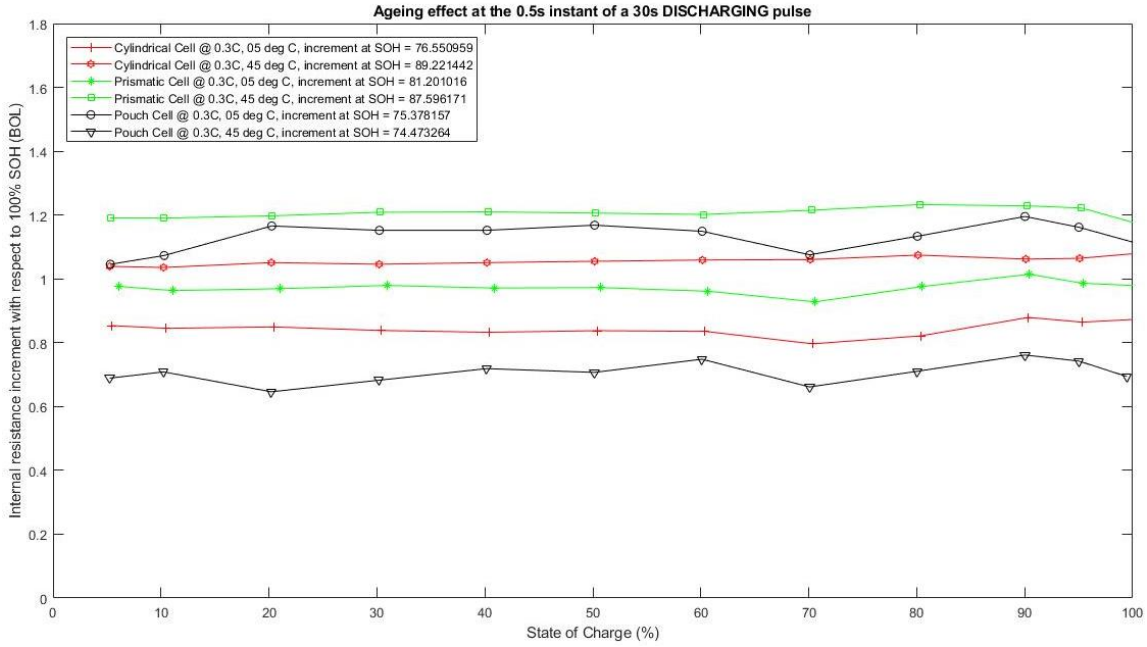

Figure 5.9. Incremental internal resistance (compared to 100% SOH) at the 0.5s instant of a 30s discharging pulse.

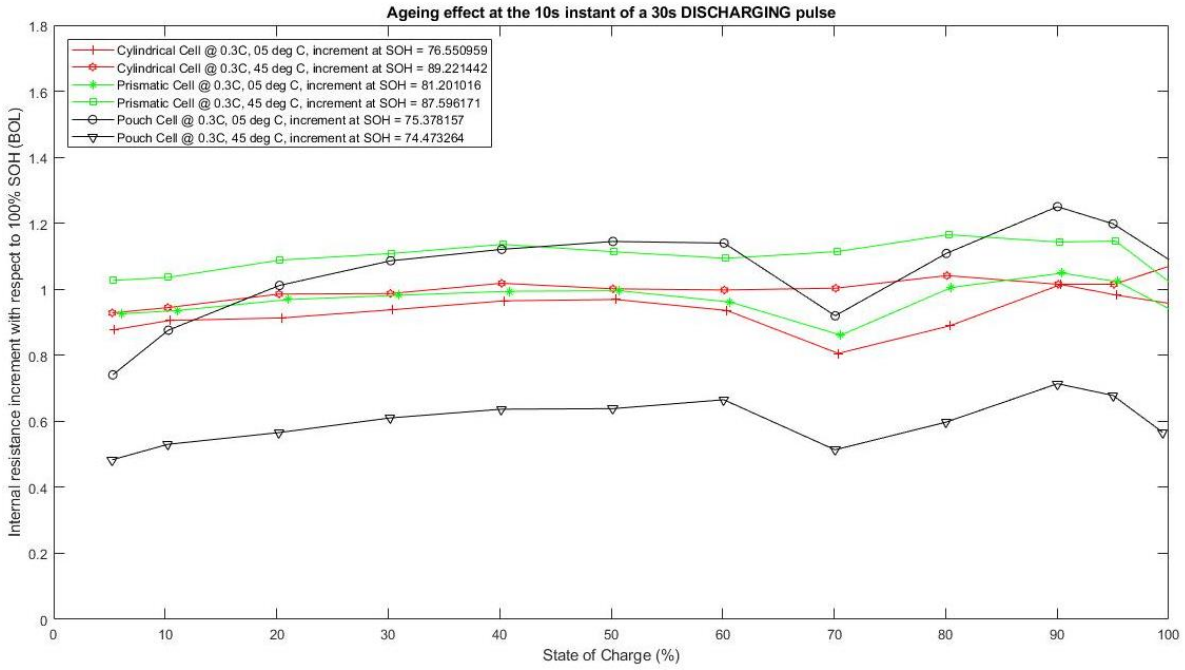

Figure 5.10. Incremental internal resistance (compared to 100% SOH) at the 10s instant of a 30s discharging pulse.

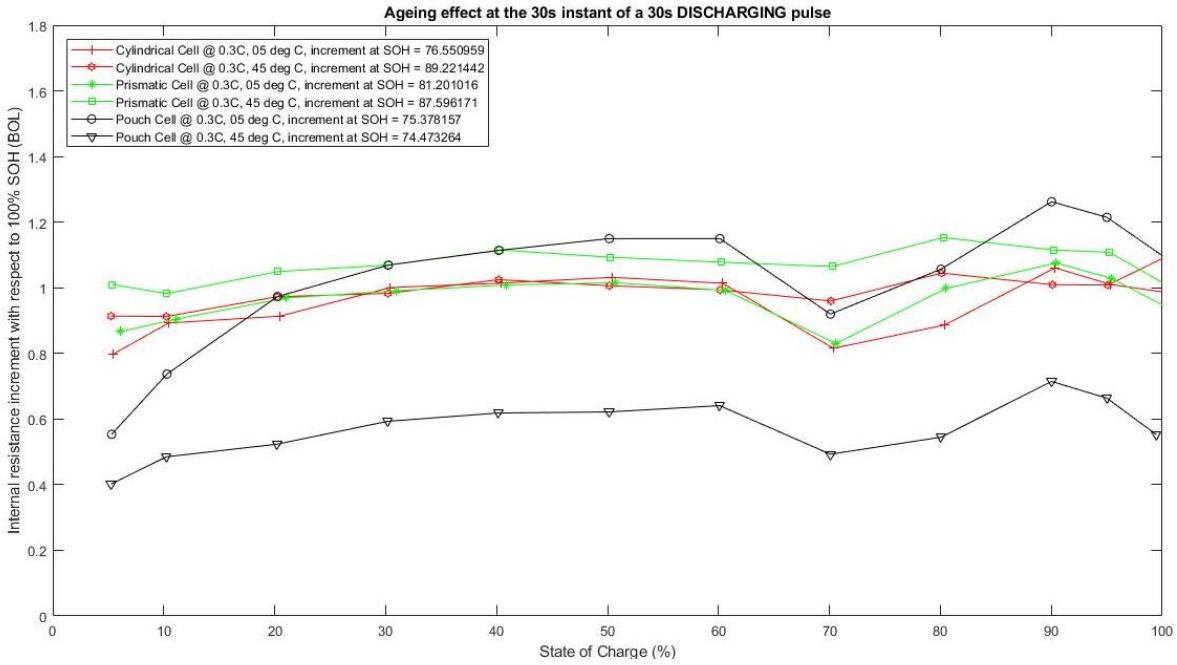

Figure 5.11. Incremental internal resistance (compared to 100% SOH) at the 30s instant of a 30s discharging pulse.

From the sections in page number 43 and page number 47, it can be inferred that the ageing of the cells can predicted based on internal resistance increment values and the effect of temperature and cycling on the equivalent cycle number and capacity drop. That is, a

decrease in internal resistance in a 30s charge/discharge test may indicate a gradual deterioration or decay of the cell life as can be seen in the case of pouch cells

NOTE: In Table 5.5 *and* Table 5.6*, the shaded rows refer to the increment ratio of the internal resistance, while the unshaded rows are the absolute values of internal resistance at the aged SOH mentioned with the geometry column. Cyl = Cylindrical, Pri = Prismatic, Po = Pouch*

	5%			**50%**			**95%**		
Pulse	*0.5s*	*10s*	*30s*	*0.5s*	*10s*	*30s*	*0.5s*	*10s*	*30s*
Charging pulse for cells at 5°C/0.3C									
Cyl	3.110	5.685	7.433	2.874	5.020	6.767	2.824	5.449	10.65
76.6%	*0.976*	***1.146***	***1.273***	*0.861*	***1.002***	***1.021***	*0.885*	*0.994*	***1.325***
Pri	3.630	5.580	6.980	3.426	5.08	6.610	3.370	5.450	9.110
81.2%	***1.081***	***1.252***	***1.196***	*0.983*	***1.104***	*0.979*	***1.005***	***1.146***	***1.087***
Po	2.244	4.393	5.867	2.296	4.149	5.649	2.325	4.608	6.750
75.4%	***1.141***	*0.633*	***1.147***	***1.139***	*0.629*	***1.083***	***1.311***	*0.708*	***1.310***
Charging pulse for cells at 45°C/0.3C									
Cy	2.877	4.666	6.125	2.820	4.325	5.804	2.657	4.193	6.544
89.2%	***1.082***	***1.202***	***1.221***	***1.126***	*0.999*	*0.990*	***1.193***	***1.091***	*0.962*
Pri	3.742	5.442	6.847	3.670	5.036	6.352	3.574	5.078	7.331
87.6%	***1.245***	***1.172***	***1.310***	***1.284***	*0.977*	***1.051***	***1.394***	***1.042***	***1.071***
Po	1.497	2.497	3.333	1.627	2.476	3.190	1.708	2.768	3.809
74.5%	*0.712*	***1.155***	*0.607*	*0.740*	***1.105***	*0.591*	*0.914*	***1.232***	*0.713*

Table 5.5. Changing in internal resistance due to ageing (for charging pulses)

	5%			**50%**			**95%**		
Pulse	*0.5s*	*10s*	*30s*	*0.5s*	*10s*	*30s*	*0.5s*	*10s*	*30s*
Discharging pulse for cells at 5°C/0.3C									
Cyl 76.55 %	3.247	6.767	10.741	2.830	4.541	6.096	2.792	4.385	5.598
	0.853	*0.877*	*0.798*	*0.837*	*0.965*	***1.031***	*0.864*	*0.982*	***1.010***
Pri 81.20 %	3.731	6.722	10.211	3.420	4.744	6.019	3.364	4.664	5.746
	0.976	*0.926*	*0.866*	*0.972*	*0.994*	***1.015***	*0.986*	***1.023***	***1.029***
Po 75.38 %	2.150	4.720	7.070	2.010	3.532	4.878	1.972	3.524	4.745
	1.045	*0.740*	*0.553*	***1.168***	***1.120***	***1.149***	***1.161***	***1.198***	***1.214***
Discharging pulse for cells at 45°C/0.3C									
Cy 89.22 %	3.029	5.641	8.909	2.748	3.991	5.221	2.701	3.858	4.901
	1.039	*0.928*	*0.913*	***1.055***	***1.018***	***1.006***	***1.064***	***1.015***	***1.008***
Pri 87.60 %	3.890	6.387	9.567	3.630	4.802	5.927	3.564	4.649	5.591
	1.190	***1.026***	***1.009***	***1.206***	***1.136***	***1.093***	***1.222***	***1.146***	***1.108***
Po 74.47 %	1.392	2.648	4.112	1.307	2.030	2.700	1.325	2.040	2.643
	0.689	*0.483*	*0.402*	*0.707*	*0.636*	*0.621*	*0.742*	*0.678*	*0.663*

Table 5.6. Changing in internal resistance due to ageing (for discharging pulses)

6 Summary and Prospect

In the last chapters the following points will be discussed:

- Summary of the results achieved and important conclusions
- Reference to the task
- Prospect: Which questions could not be processed within the scope of this work? Where there is still room for improvement in the thematic environment and what are the chances of development in the future?

It may be useful to keep these two chapters separately.

Bibliography

[1]SPICY Innovative Battery. 2015. Silicon and polyanionic chemistries and architectures of Li-ion cell for high energy battery. CEA GRENOBLE (2015). http://www.spicy-project.eu/.

[2]Buchmann, Isidor. 2018. BU-1003: Electric Vehicle (EV). Battery University, Cadex Electronics Inc (2018). https://batteryuniversity.com/index.php/learn/article/electric_vehicle_ev.

[3]Grandjean, Thomas; Barai, Anup; Hosseinzadeh, Elham; Guo, Yue; McGordon, Andrew; Marco, James. 2017. Large format lithium ion pouch cell full thermal characterisation for improved electric vehicle thermal management (2017). Journal of Power Sources. 359.

[4]Erriquez, Mauro; Morel, Thomas; Schäfer, Philip; Moulière, Pierre-Yves. October 2017. Trends in electric-vehicle design. McKinsey&Company, Automotive & Assembly (October 2017). https://www.mckinsey.com/industries/automotive-and-assembly/our-insights/trends-in-electric-vehicle-design.

[5]Alarco, Jose; Talbot, Peter. 2015. The history and development of batteries (2015). https://phys.org/news/2015-04-history-batteries.html#jCp.

[6]Blomgren, George E. 2016. The Development and Future of Lithium Ion Batteries (2016). Journal of The Electrochemical Society. 164.

[7]Nitta, Naoki; Wu, Feixiang; Lee, Jung Tae; Yushin, Gleb. 2015. Li-ion battery materials (2015). Materials Today. 18.

[8]Saha, Bhaskar; Goebel, Kai (2009). Modeling Li-ion battery capacity depletion in a particle filtering framework. https://pdfs.semanticscholar.org/6da6/f559425e9b9f719be1089b3cf254dcc1f8d0.pdf.

[9]Soylu, Seref. 2011. Electric Vehicles â€“ The Benefits and Barriers. 978-953-307-287-6.

[10]Buchmann, Isidor. 2018. BU-205: Types of Lithium-ion. Battery University, Cadex Electronics Inc (2018). http://batteryuniversity.com/learn/article/types_of_lithium_ion.

[11]Padhi, A. K. 1997. Phospho-olivines as Positive-Electrode Materials for Rechargeable Lithium Batteries (1997). Journal of The Electrochemical Society. 144.

[12]Eftekhari, Ali. 2017. LiFePO 4 /C nanocomposites for lithium-ion batteries (2017). Journal of Power Sources. 343.

[13]Athena Combs-Hurtado; Marc Hensel. Memorandum: Using Lithium Iron Phosphate Batteries for Utility Scale Storage Applications. Arizona State University (21 October 2017). http://roedel.faculty.asu.edu/sec598s18/projects/p01_SM.pdf.

[14]Zhang, Xiangwu; Ji, Liwen; Toprakci, Ozan; Liang, Yinzheng; Alcoutlabi, Mataz. 2011. Electrospun Nanofiber-Based Anodes, Cathodes, and Separators for Advanced Lithium-Ion Batteries (2011). Polymer Reviews. 51.

[15]Schröder, Robert; Aydemir, Muhammed; Seliger, Günther. 2017. Comparatively Assessing different Shapes of Lithium-ion Battery Cells (2017). Procedia Manufacturing. 8.

[16]Buchmann, Isidor. 2018. BU-301a: Types of Battery Cells. Battery University, Cadex Electronics Inc (2018). http://batteryuniversity.com/learn/article/types_of_battery_cells.

[17]Jessica Shankleman; Tom Biesheuvel; Joe Ryan; Dave Merrill. 2017. We're Going to Need More Lithium. Bloomberg LP (2017). https://www.bloomberg.com/graphics/2017-lithium-battery-future/.

[18]AUDI Digital Illustrated. 2016. AUDI future performance 2015 illustrated. AUDI Illustrated (2016). https://www.audi-illustrated.com/en/future-performance-2015/Batterietechnologie.

[19]Jaggi, Anmol. Jan 26, 2017. Comparison of different Li-ion cell types. Gensol Engineering Pvt. Ltd. (Jan 26, 2017). https://www.slideshare.net/AnmolJaggi/comparison-between-different-li-ion-cells-type.

[20]Ahn, Soonho; Lee, Hyang-Mok; Lee, Seung-Jin; Youngsun, Park; Ku, Cha-Hun; Kim, Je Young; Lee, Jae-Hyun; Kim, Seok Koo; Cho, Jin Yeon. The Impact of Cell Geometries and Battery Designs on Safety and Performance of Lithium Ion Polymer Batteries. Batteries R&D, LG Chemical Ltd./ Research Park. https://www.electrochem.org/dl/ma/203/pdfs/0106.pdf.

[21]Maiser, Eric (2014). Battery packaging - Technology review.

[22]Mulder, Grietus; Omar, Noshin; Pauwels, Stijn; Meeus, Marcel; Leemans, Filip; Verbrugge, Bavo; Nijs, Wouter de; van den Bossche, Peter; Six, Daan; van Mierlo, Joeri. 2013. Comparison of commercial battery cells in relation to material properties (2013). Electrochimica Acta. 87.

[23]Zhao, Jingyuan. 2018. Cycle life testing of lithium batteries (2018). International Journal of Electrochemical Science.

[24]Anseán González, David. 2015. High power li-Ion battery performance: a mechanistic analysis of aging (2015).

[25]Barré, Anthony; Deguilhem, Benjamin; Grolleau, Sébastien; Gérard, Mathias; Suard, Frédéric; Riu, Delphine. 2013. A review on lithium-ion battery ageing mechanisms and estimations for automotive applications (2013). Journal of Power Sources. 241.

[26]Sarasketa-Zabala, E.; Gandiaga, I.; Martinez-Laserna, E.; Rodriguez-Martinez, L. M.; Villarreal, I. 2015. Cycle ageing analysis of a LiFePO 4 /graphite cell with dynamic model validations (2015). Journal of Power Sources. 275.

[27]Pinson, M. B.; Bazant, M. Z. 2012. Theory of SEI Formation in Rechargeable Batteries (2012). Journal of the Electrochemical Society. 160. https://arxiv.org/ftp/arxiv/papers/1210/1210.3672.pdf.

[28]Sikha, G.; Ramadass, P.; Haran, B. S.; White, R. E.; Popov, Branko N. 2003. Comparison of the capacity fade of Sony US 18650 cells charged with different protocols (2003). Journal of Power Sources. 122.

[29]Han, Xuebing; Ouyang, Minggao; Lu, Languang; Li, Jianqiu; Zheng, Yuejiu; Li, Zhe. 2014. A comparative study of commercial lithium ion battery cycle life in electrical vehicle (2014). Journal of Power Sources. 251.

[30]Sun, Shun; Guan, Ting; Shen, Bin; Leng, Kunyue; Gao, Yunzhi; Cheng, Xinqun; Yin, Geping. 2017. Changes of Degradation Mechanisms of LiFePO 4 /Graphite Batteries Cycled at Different Ambient Temperatures (2017). Electrochimica Acta. 237.

[31]Lewerenz, Meinert; Marongiu, Andrea; Warnecke, Alexander; Sauer, Dirk Uwe. 2017. Differential voltage analysis as a tool for analyzing inhomogeneous aging (2017). Journal of Power Sources. 368.

[32]Frank Kindermann. 2012. The Solid-Electrolyte Interface.

[33]DuBeshter, Tyler; Jorne, Jacob. 2017. Pulse Polarization for Li-Ion Battery under Constant State of Charge (2017). Journal of The Electrochemical Society. 164.

[34]Liu, Chaofeng; Neale, Zachary G.; Cao, Guozhong. 2016. Understanding electrochemical potentials of cathode materials in rechargeable batteries (2016). Materials Today. 19. https://www.sciencedirect.com/science/article/pii/S1369702115003181.

[35]Park, Myounggu; Zhang, Xiangchun; Chung, Myoungdo; Less, Gregory B.; Sastry, Ann Marie. 2010. A review of conduction phenomena in Li-ion batteries (2010). Journal of Power Sources. 195.

[36]Zhou, Daming; Zhang, Ke; Ravey, Alexandre; Gao, Fei; Miraoui, Abdellatif. 2016. Parameter Sensitivity Analysis for Fractional-Order Modeling of Lithium-Ion Batteries (2016). Energies. 9.

[37]Gamry Instruments. 2018. Testing lithium ion batteries. Gamry Instruments (2018). https://www.gamry.com/application-notes/battery-research/testing-lithium-ion-batteries/.

[38]Yaakov, David; Gofer, Yossi; Aurbach, Doron; Halalay, Ion C. 2010. On the Study of Electrolyte Solutions for Li-Ion Batteries That Can Work Over a Wide Temperature Range (2010). Journal of The Electrochemical Society. 157.

[39]Palcoux, G.; Schmalz, J.; Richter, L.; Porcher, W. SPICY Deliverable D5.6. CEA, TUM-PROLLION.

[40]BaSyTec GmbH. BaSyTec XCTS. BaSyTec GmbH.

[41]Trad, Khiem; Mulder, Grietus; Gutiérrez, César; Meatza, Iratxe de; Delaille, Arnaud; Porcher, Willy. SPICY Deliverable D6.1. CIDETEC, CEA, TUM, PROLLION.

[42]M. Nisvo Ramadan; Bhisma A. Pramana; Adha Cahyadi; Oyas Wahyunggoro. 2016. State of health estimation in lithium polymer battery.

[43]Li, Lian-xing; Tang, Xin-cun; Qu, Yi; Liu, Hong-tao. 2011. CC-CV charge protocol based on spherical diffusion model (2011). Journal of Central South University of Technology. 18.

[44]Svens, Pontus; Behm, Mårten; Lindbergh, Göran. 2015. Lithium-Ion Battery Cell Cycling and Usage Analysis in a Heavy-Duty Truck Field Study (2015). Energies. 8.

[45]Liu, Guang; Guo, Liang; Liu, Chunlong; Wu, Qingwen. 2018. Evaluation of different calibration equations for NTC thermistor applied to high-precision temperature measurement (2018). Measurement. 120.

[46]Chang, Wen-Yeau. 2013. The State of Charge Estimating Methods for Battery (2013). ISRN Applied Mathematics. 2013.

[47]Zhao, Rui; Zhang, Sijie; Gu, Junjie; Liu, Jie. 2016. 2016 IEEE Electrical Power and Energy Conference (EPEC). IEEE Electrical Power and Energy Conference; Annual IEEE Electrical Power and Energy Conference; Conférence sur l'énergie électrique de l'IEEE; EPEC. 978-1-5090-1919-9.

[48]Novais, Susana; Nascimento, Micael; Grande, Lorenzo; Domingues, Maria Fátima; Antunes, Paulo; Alberto, Nélia; Leitão, Cátia; Oliveira, Ricardo; Koch, Stephan; Kim, Guk Tae; Passerini, Stefano; Pinto, João. 2016. Internal and External Temperature Monitoring of a Li-Ion Battery with Fiber Bragg Grating Sensors (2016). Sensors (Basel, Switzerland). 16.

[49]An, Seong Jin; Li, Jianlin; Daniel, Claus; Mohanty, Debasish; Nagpure, Shrikant; Wood, David L. 2016. The state of understanding of the lithium-ion-battery graphite solid electrolyte interphase (SEI) and its relationship to formation cycling (2016). Carbon. 105.

[50]Wu, Yao; Keil, Peter; Schuster, Simon F.; Jossen, Andreas. 2017. Impact of Temperature and Discharge Rate on the Aging of a LiCoO 2 /LiNi 0.8 Co 0.15 Al 0.05 O 2 Lithium-Ion Pouch Cell (2017). Journal of The Electrochemical Society. 164.

List of Figures

List of Tables